~~CONFIDENTIAL~~

Copy 227
RM L55H22b

NACA RM L55H22b

NACA
RM
L55H22B
c.227

TECH LIBRARY KAFB, NM
0069384

NACA

RESEARCH MEMORANDUM

INITIAL EXPERIMENTAL INVESTIGATION OF THE AERODYNAMIC LOAD ON THE WING OF A MODEL CAUSED BY A BLAST-INDUCED GUST THAT INCREASES THE ANGLE OF ATTACK INTO THE STALL REGION

By Harold B. Pierce and Thomas D. Reisert

Langley Aeronautical Laboratory
Langley Field, Va.

Declassified by Authority of LARC Security Classification Officer (SCO) Letter dated June 16, 1983
M Beard Johnson

[redacted]

This material contains information affecting the National [redacted] of the espionage laws, [redacted] Sections 793 and 794, the transmission or revelation of which in any [redacted] unauthorized person is prohibited by law.

NATIONAL ADVISORY COMMITTEE FOR AERONAUTICS

WASHINGTON
December 19, 1955

~~CONFIDENTIAL~~

8600

FILE

National Aeronautics and
Space Administration

Langley Research Center
Hampton, Virginia
23665

NASA

Reply to Attn of: 139A

JUN 1 6 1983

TO: Distribution

FROM: 180A/Security Classification Officer

SUBJECT: Authority to Declassify NACA/NASA Documents Dated Prior to January 1, 1960

Effective this date, all material (informal, correspondence) classified by this Center prior to January 1, 1960, is declassified. This action does not include material derivatively classified at the Center upon instructions from other Agencies.

Immediate re-marking is not required; however, until material is re-marked by lining through the classification and annotating with the following statement, it must continue to be protected as if classified:

> "Declassified by authority of LaRC Security Classification Officer (SCO) letter dated June 16, 1983," and the signature of person performing the re-marking.

If re-marking a large amount of material is desirable, but unduly burdensome, custodians may follow the instructions contained in NHB 1640.4, subpart F, section 1203.604, paragraph (h).

This declassification action complements earlier actions by the National Archives and Records Service (NARS) and by the NASA Security Classification Officer (SCO). In Declassification Review Program 807008, NARS declassified the Center's "Research Authorization" files, which contain reports, Research Authorizations, correspondence, photographs, and other documentation. Earlier, in a 1971 letter, the NASA SCO declassified all NACA/NASA formal series documents with the exception of the following reports, which must remain classified:

Document No.	First Author
E-51A30	Nagey
E-53G20	Francisco
E-53G21	Johnson
E-53K18	Spooner
SL-54J21a	Westphal
E-55C16	Fox
E-56H23a	Himmel

JUN 2 3 1983

05-05-1997 11:29 804 864 2375 LARC TECH LIBRARY P.02

If you have any questions concerning this matter, please call Mr. William L. Simkins at extension 3281.

Jess G. Ross
2898

Distribution:
SDL 031

cc:
NASA Scientific and Technical
Information Facility
P.O. Box 8757
BWI Airport, MD 21240

NASA--NIS-5/Security
180A/RIAD
139A/TU&AO

139A/WLSimkins:elf 06/15/83 (3281)

139A/JS 6-15-83

31-01 HEADS OF ORGANIZATIONS
HESS, JANE S.,
MAIL STOP 185 BLDG 1194

0069384

NATIONAL ADVISORY COMMITTEE FOR AERONAUTICS

RESEARCH MEMORANDUM

INITIAL EXPERIMENTAL INVESTIGATION OF THE AERODYNAMIC LOAD ON THE WING OF A MODEL CAUSED BY A BLAST-INDUCED GUST THAT INCREASES THE ANGLE OF ATTACK INTO THE STALL REGION

By Harold B. Pierce and Thomas D. Reisert

SUMMARY

An initial experimental investigation has been completed on the aerodynamic load imposed on the wing of an airplane model by a blast-induced gust which increased the angle of attack well beyond the stall angle. Pressure distributions at intervals of 1 millisecond were derived from time histories of resultant pressure measured at 10 stations along the wing chord. Comparison of these distributions with distributions obtained from steady-flow wind-tunnel tests and potential-flow calculations showed that neither of the latter methods was adequate to predict the loads in the transient conditions of the blast. A traveling peak of negative pressure was disclosed that is believed to be of significance for the high angle-of-attack case. It was attributed to a vortex formed by the diffraction of the blast wave around the wing. The normal-force coefficients obtained from the flight pressure distributions were approximately twice those predicted from wind-tunnel tests for the first 12 milliseconds after blast arrival or for about 75 percent of the time the angle of attack was above the stall.

INTRODUCTION

A blast-induced gust is highly transient and produces extremely rapid changes in angle of attack of the wing that may go well beyond the stall angle. Attempts to estimate lift and moment under such conditions of transient flow by the use of steady-flow theory and experiment, as well as the selection of unsteady-lift functions for some of the conditions, would certainly be of doubtful success. As a result of these uncertainties, the NACA has inaugurated experiments with airplane models subjected to actual blast-induced gusts to obtain information on the maximum lift coefficients attainable when the angle of attack goes beyond the steady-flow stall angle and on the proper

selection of the unsteady-lift function when separation does not occur. The experimental work is performed at Wallops Island, Va.

The purpose of this report is to present the first pressure-distribution data obtained during preliminary experiments made primarily to develop techniques and establish the reliability of the results. These data were obtained during three repeat flights to examine maximum lift for the condition in which the blast-induced gust initially increased the angle of attack about four times above the steady-flow stall angle of the model. The large angle-of-attack change was chosen to insure that not only would the maximum angle of attack in the gust be in the steady-flow stall region for the model, but that it also would be at least twice the stall angle for the full-scale wing section.

SYMBOLS

C_D	drag coefficient
C_L	lift coefficient
C_M	pitching-moment coefficient
C_N	normal-force coefficient
Δp	resultant pressure, lb/sq in.
q	dynamic pressure, lb/sq in.
U	gust velocity, ft/sec
V	forward velocity, ft/sec
α	angle of attack, deg

TEST PROCEDURE

The procedure used in the experiments consists of launching a model into free flight by use of a rocket and subjecting it to a gust induced

by the blast wave from a charge of high explosive. Pressures at 10 stations on the model can be recorded by a telemetering system and the resultant pressure distributions are compared with wind-tunnel measurements and the results of steady-flow calculations. Measurements of the time history of blast pressure near the model and of the forward velocity, positions, and attitude of the model are used to define the test conditions at blast encounter. All pressures obtained in the tests were measured as increments from the pressures existing on the gages less than 1 millisecond before the blast wave struck.

APPARATUS AND INSTRUMENTS

Blast Area and Major Equipment

The area at which the tests are conducted is located in the sand dunes north of the Langley Pilotless Aircraft Research Station at Wallops Island, Va., and consists of a control center housed in a trailer, blast gages suitably mounted on poles to determine the blast overpressure, camera targets, and three fixed camera stations used to record the model speed, position, and attitude. The general layout is shown in figure 1. The control center in the trailer contains the ground telemeter station, the test programer, blast-pressure recorders, timers, and equipment for making final adjustments to the telemeter in the model.

Model

The configuration of the model used in the tests was chosen primarily because previous experience had shown it to have good flying qualities. It is a 1/20-scale model of a DC-4 airplane modified to the extent that the fuselage is a body of revolution and that the wing is mounted at zero incidence and has an NACA 0009-64 section. A photograph of the model is shown in figure 2 and a three-view line drawing in figure 3. The characteristics of the model are as follows:

Weight, W, lb	31.56
Wing area, S, sq ft	3.72
Wing loading, W/S, lb/sq ft	8.48
Span, b, ft	5.95
Mean geometric chord, ft	0.626
Aspect ratio, b^2/S	9.51
Airfoil section	NACA 0009-64
Center-of-gravity position, percent mean chord	22
Pitching moment of inertia, slug-ft^2	0.619

As indicated in the side view in figure 3, the model was propelled by a modified $2\frac{1}{4}$-inch aircraft rocket mounted in the aft end of the fuselage. A parachute was mounted in the fairing below the wing to aid in retrieving the model after the test.

The model was constructed of glass cloth and plastic and was designed to withstand launching and landing loads rather than to have scaled structural characteristics or weight. The wing was of built-up construction with balsa ribs and thick glass-cloth and plastic skin except at the wing station 17.87 inches from the center line of the fuselage, where a solid rib was provided to encase 10 NACA miniature electrical pressure gages. The gages were arranged as shown in figure 4 to measure resultant pressures at orifice locations from 5 to 84 percent of the chord. The channels from the orifices to the gages were made of equal length to minimize differences in response characteristics. For the first of the three flights, all of the gages were encased in a single solid rib of plastic, but preliminary flights had loosened the seal around the gages so that only five were reliable at the time of the flight. The plastic rib was removed and a split aluminum rib with provisions for better sealing was inserted for the subsequent flights.

Instrumentation

The pressure gages in the wing were in individual oscillator circuits whose frequency changed when pressure was applied to the gages. In turn, these separate frequencies modulated an FM signal which was transmitted by trailing wire to the ground receiving station. The FM signal was unscrambled into 10 individual outputs that were recorded simultaneously on a tape recorder of 14-channel capacity, and after the test the channels were played back individually onto oscillograph records. The complete system has a response that is essentially flat to 500 cycles per second and that is useful to 1,000 cycles per second.

Two fixed cameras (fig. 1) were used to record the speed, attitude, and position of the model. The cameras were operated at about 20 frames per second and recorded the position of the model on 70-mm film. Both cameras were 140 feet from the launching position of the model. They were at the same level and the axes of both were elevated at an angle of 15° with the horizontal. At each shutter opening, a mark was recorded on 35-mm film in a strip camera in the control center. On the same film, 500-cps timing was recorded, together with synchronization pulses which tied the camera frames to the other records within an accuracy of 2 milliseconds.

Blast gages located as shown in figure 1 were used to measure the side-on pressure due to each blast. An NACA miniature electrical pressure

gage mounted, as shown in figure 5, in the center of an aluminum disk 18 inches in diameter and 1/8 inch thick comprised the blast gage. The units were mounted at an angle of 5° with the blast as suggested in reference 1 to reduce boundary-layer effects. The pressure gages were in a bridge circuit utilizing a 25-kc carrier system. The output of the system was directed to a four-beam oscilloscope and to the tape recorder. Photographs of the face of the oscilloscope, taken by a 35-mm strip camera, recorded the output of the two blast gages as well as synchronization marks and 1,000-cps timing. The blast-measuring system had a rise time of 1 millisecond.

Timing and Synchronization

A 1,000-cps tuning-fork oscillator was used as the primary source for timing on all records. Synchronization pulses were sent to each record at 1/10-second intervals, starting within 1/10 second after firing the model. Although timing could not be impressed directly on the 70-mm movie film, the synchronization pulses flashed a neon bulb in these cameras and also on the film of the associated strip camera. When the shutter of the movie camera was open at the time that the bulb flashed, a mark was made on a small portion of that frame. Comparison of these marks with those made on the strip camera referenced the movie frames to the other records.

Programer

Since a number of functions, such as operation of the recorders and cameras and firing of the model and blast, had to be performed within a short time interval, a programer was provided to take over the operations on a signal from a remote position. The programer can perform an operation at any of the steps available - that is, at -60, -45, -30, and -15 seconds and every second thereafter to +9 seconds - so that the individual operations can occur in different sequences depending on test requirements. The blast must be fired so that the blast wave strikes the model when it is in a given position, and the time steps provided in the programer itself are too coarse to provide the precise timing required. Accordingly, the rocket in the model is fired at the zero time step on the programer, and when the model leaves the ground it breaks a circuit which activates a delay timer. This timer is set for the time interval equal to the rocket burning time minus the time required for the blast wave to reach the model, and it fires the blast when the interval has elapsed. An overriding safety switch is provided so that in the event of trouble, the operations can be stopped at any time.

TESTS

Three flights were made at a velocity of about 110 feet per second. The model was trimmed for zero lift and launched at 11° with the vertical. The launching angle was selected so that at rocket burnout the model would be flying tangent to the shock front and the gust or material velocity would be normal to the flight path, as illustrated in figure 6. On the first flight, five channels of pressure information from the stations at 5, 12, 19, 68, and 84 percent of the chord were obtained, while all 10 channels were available for the last two flights.

Blast-induced gusts having maximum velocities of about 76 feet per second were produced by the explosion of hemispherical charges of composition C-3 weighing 150 pounds. The charges were mounted 5.31 feet above the ground and about 200 feet from the point of tangency of the flight path of the model with the resultant shock front. Preliminary tests showed that, with the charge located in this manner, the model would be in the Mach stem region and be subjected to a single shock front with the resulting gust closely approximating that from a 300-pound charge exploded in free air. The time histories of gust velocity were determined by Rankine-Hugoniot shock-wave equations from estimations of the blast overpressure at the model obtained from the time histories of overpressure shown in figure 7. For the conditions of this test (overpressures well below 7 lb/sq in.), these equations closely describe the flow behind the shock. The locations of the gages with respect to the blasts are also given in the figure and it should be noted that only one gage was operative for flights 1 and 3, while both gages gave records in flight 2. The records shown were faired to eliminate gage ringing. Knowing the variation of overpressure with distance from the explosion point, which can be determined from curves of the type shown in reference 2, the overpressure variation at the model could be estimated. In table I, the conditions at the time of blast-wave arrival are summarized for each flight.

In addition to the free-flight tests, a wind-tunnel investigation was made in the Langley 300 MPH 7- by 10-foot tunnel to obtain the steady-flow pressure distributions over the test wing chord for angles of attack from 0° to 45°. These tests were made at the same speed as the flight speed, but upper- and lower-surface pressures were measured separately at 14 stations along the chord. Data were obtained every 2° up to an angle of attack of 18° and then every 4° to an angle of attack of 45°. Lift, drag, and moment of the entire model were also obtained for the same angle-of-attack range and the results in coefficient form are presented in figure 8.

PRECISION

The measured quantities are estimated to be accurate within the following limits for any test or run:

Forward velocity, ft/sec	±3
Overpressure, percent	±5
Differential pressure on model, percent	±5
Angle of attack, deg	±2

The first 2 milliseconds of the wing pressure records after blast arrival are not considered to be of much value since the measuring system is usable only to frequencies of 1,000 cps.

The angle-of-attack variation, determined basically from the variation in gust velocity, was corrected for wing flexibility and model motion by calculations involving the weight and pitching moment of the model and the fundamental bending frequency of the wing. The angle-of-attack variation caused by the gust, as obtained in one test, is shown as the solid line in figure 9. The dashed line in the figure represents the estimated actual angle-of-attack change at the measuring station, obtained by subtracting the calculated angle-of-attack change due to the motions of this station from the gust-angle change. Since the effects of the motions of the model are small, errors due to the approximations made in the calculations have little effect, particularly in the early portions of the time history where the gust angle is large.

RESULTS AND DISCUSSION

Time histories of the differential pressure at each active gage station on the wing were evaluated for each flight. A sample time history for the 37-percent-chord station is shown in figure 10. Chordwise distributions of the resultant pressure coefficients were obtained from the time histories of resultant pressure at each gage station for each flight. These distributions are presented in figures 11(a) to 11(r) at increments of 1 millisecond, starting 3 milliseconds after blast arrival. The values of dynamic pressure used in computing the pressure coefficients from the pressure results were based on the resultant velocity and air density caused by the blast-induced gust. In the present case the gust caused an initial instantaneous increase in the dynamic pressure of about 45 percent. The values given in the figure legends for angle of attack and distance traveled after blast arrival are averages for the three flights.

Examination of figure 11 shows that the results from the three flights are consistent to the degree that the reliability of the technique

is believed established. Except in figures 11(g) and 11(h), where there are obviously some questionable data points for flights 2 and 3, a region of high negative pressure coefficient is indicated which moves along the chord with time and passes beyond the range of the rearmost measuring point after about 18 milliseconds have elapsed. During this time the airfoil has moved forward 3.2 chord lengths, so it is apparent that the movement of the pressure area was not directly related to the forward speed of the model. This moving pressure region is believed to be of significance for the high angle-of-attack case. It is thought to be due to the influence of a vortex passing over the upper surface of the wing. This vortex, in turn, is believed to be formed at the leading edge on the upper surface of the airfoil by the diffraction of the shock wave as it passes over the airfoil in a direction normal to the chord line of the wing. This premise is based in part on shock-tube investigations of the type reported in reference 3, where interferograms show the formation of a vortex when a shock wave passes over a bluff body.

Single pressure distributions for each millisecond after blast arrival were obtained by simple averaging of the data from the three flights. For comparison with these experimental results, pressure distributions for steady-flow conditions were determined from the wind-tunnel tests for the corresponding angles of attack. In addition, pressure distributions were calculated for each angle of attack by the method of reference 4 from data given in reference 5. This method utilizes potential-flow concepts and the results represent the pressure distributions for the unstalled condition with the flow remaining attached to the airfoil. The two-dimensional slope of the lift curve, 2π per radian, was used in the calculations. No consideration was given to unsteady lift in the calculations. Figures 12(a) to 12(r) present the pressure distributions obtained by the three different methods and show that the flight results are not predicted by either the wind-tunnel investigation or the potential-flow calculations. It appears that the traveling vortex modifies the flow over the wing so that neither the separated flow indicated by wind-tunnel tests nor the attached flow assumed in the calculations predominates. Inspection of the figure shows that the maximum value of the pressure coefficient due to the vortex is always above the potential-flow line.

Normal-force coefficients on the wing chord investigated were determined by integration of the resultant pressure-coefficient distributions of figure 12. The results are shown in figure 13 plotted against angle of attack. The time sequence of the curves is from high to low angle of attack, and the points for the flight data which start 3 milliseconds after blast arrival are separated by time intervals of 1 millisecond. For about 12 milliseconds after blast arrival, the normal-force coefficient is about twice that obtained from the wind-tunnel tests. The flight data then fall off until they are below the wind-tunnel data, and they cross the zero axis while there is still an indicated angle of attack of about 4°.

A possible explanation for the large differences noted in figure 13 between the flight tests and wind-tunnel tests is that the flow on the upper surface of the wing lags behind the change in angle of attack. Since steady flow exists on the wing before it is struck by the blast gust, about 3 chord lengths of travel are required for complete separation to occur (assuming the pressure peak to be associated with the separation). During this time, it seems reasonable that the load is higher than the wind-tunnel data, where complete separation exists for the same angle of attack. Just about the time that the separation is complete, the angle of attack falls below the wind-tunnel stall angle and, since the flow is separated and must reattach itself, the load is less than the unstalled wind-tunnel data.

Figure 14 presents the moment coefficients about the quarter-chord point of the airfoil as a function of angle of attack, as determined from the flight and wind-tunnel tests. Once again the time sequence is from right to left. It is immediately apparent that the flight results differ considerably from the wind-tunnel results both in magnitude and direction. The effect of the traveling high negative pressure area is shown at the high angles of attack by the fact that the curve first indicates positive moments and then crosses over to negative moments as the pressure region moves aft. As a matter of interest, the moment coefficients are also shown in figure 15 plotted against the normal-force coefficient.

In the application of the results of these tests to conditions of larger scale and higher speeds, certain reservations must be kept in mind. Perhaps the most important of these is the question of similarity of the vortex formation when the blast wave is diffracted around the airfoil under the new conditions. In the present case a vortex apparently was formed, but additional tests will be required to establish the parameters governing its formation and strength. Until such time as test results are available, shock-tube investigations such as described in references 6 and 7 may be used to gain some idea of the influence of Reynolds number and changes in shock strength on the vortex formation over sharp-edged bodies.

CONCLUDING REMARKS

The results of the low-speed investigation to determine the pressure distribution on one chord of a wing for an angle-of-attack change to about four times the angle at stall, caused by a blast-induced gust, showed that steady-flow wind-tunnel tests and potential-flow calculations are inadequate to predict the loads for this condition. For the first 12 milliseconds after blast arrival, or for about 75 percent of the time the angle of attack was above the stall, the normal-force coefficient was about twice that predicted by wind-tunnel tests. A traveling

peak of pressure was found that was attributed to a vortex caused by the diffraction of the blast wave around the wing. Further tests will be required to establish the parameters governing the formation and strength of this vortex and to determine if it is important at higher speeds and Reynolds numbers.

Langley Aeronautical Laboratory,
National Advisory Committee for Aeronautics,
Langley Field, Va., August 9, 1955.

REFERENCES

1. Shreve, James D., Jr.: Orientation of Gauge Baffles in Overpressure Measurements. Ref. Sym. 5111(68), Sandia Corp. (Albuquerque, N. Mex.), Sept. 2, 1952.

2. Curtis, Wesley: Free Air Blast Measurements on Spherical Pentolite. Memo. Rep. No. 544, Ballistic Res. Labs., Aberdeen Proving Ground, July 1951.

3. Bleakney, Walker: Shock Loading of Rectangular Structures. Tech. Rep. II-11 (Contract N6ori-105 Task II), Dept. of Phys., Princeton Univ., Jan. 1952.

4. Abbott, Ira H., Von Doenhoff, Albert E., and Stivers, Louis S., Jr.: Summary of Airfoil Data. NACA Rep. 824, 1945. (Supersedes NACA WR L-560.)

5. Loftin, Laurence K., Jr., and Cohen, Kenneth S.: Aerodynamic Characteristics of a Number of Modified NACA Four-Digit-Series Airfoil Sections. NACA TN 1591, 1948.

6. Griffith, W. C., Weimer, D. K., Brickl, D. E., and Bleakney, Walker: The Effect of Reynolds Number on the Diffraction of a Shock Wave. Tech. Rep. II-8 (Contract N6ori-105 Task II), Dept. of Phys., Princeton Univ., Feb. 1951.

7. Hollyer, Robert N., Jr., and Duff, Russell E.: Growth of the Turbulent Region at the Leading Edge of Rectangular Obstacles in Shock Wave Diffraction. Rep. 51-2 (Project M720-4, Contract No. N6-ONR-232 Task Order IV), Eng. Res. Inst., Univ. of Michigan, Jan. 18, 1951.

TABLE I.- TEST CONDITIONS

	Flight 1	Flight 2	Flight 3
Maximum overpressure, lb/sq in.	1.40	1.43	1.43
Maximum gust velocity, ft/sec	75.0	76.5	76.5
Angle between flight path and gust, deg . .	90	90	90
Forward velocity of model, ft/sec	115	111	107.5
Maximum angle-of-attack change, deg	33.1	34.6	35.4
Duration of gust, milliseconds	25.2	26.2	26.2
Distance of model from blast, ft	196.3	200.0	196.3

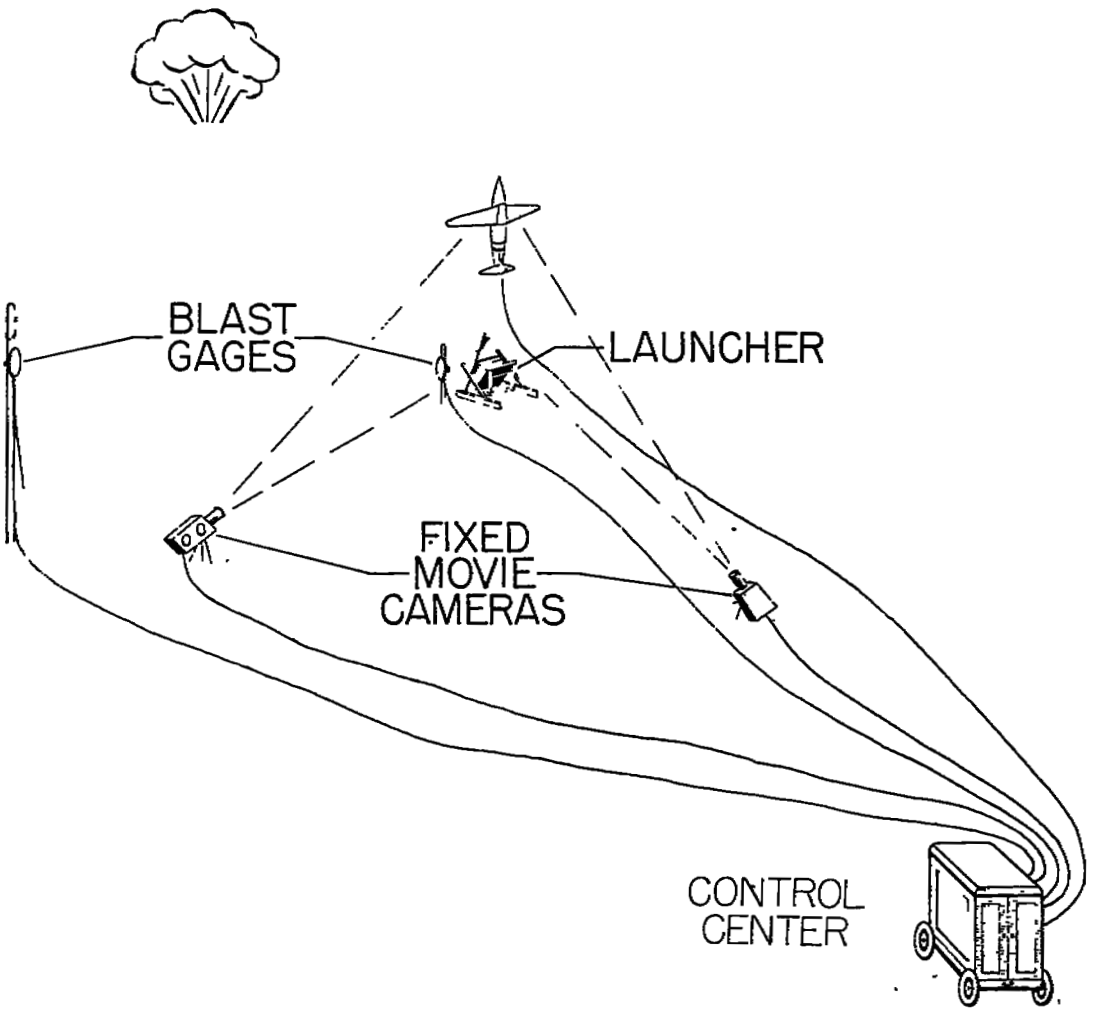

Figure 1.- General view of blast area.

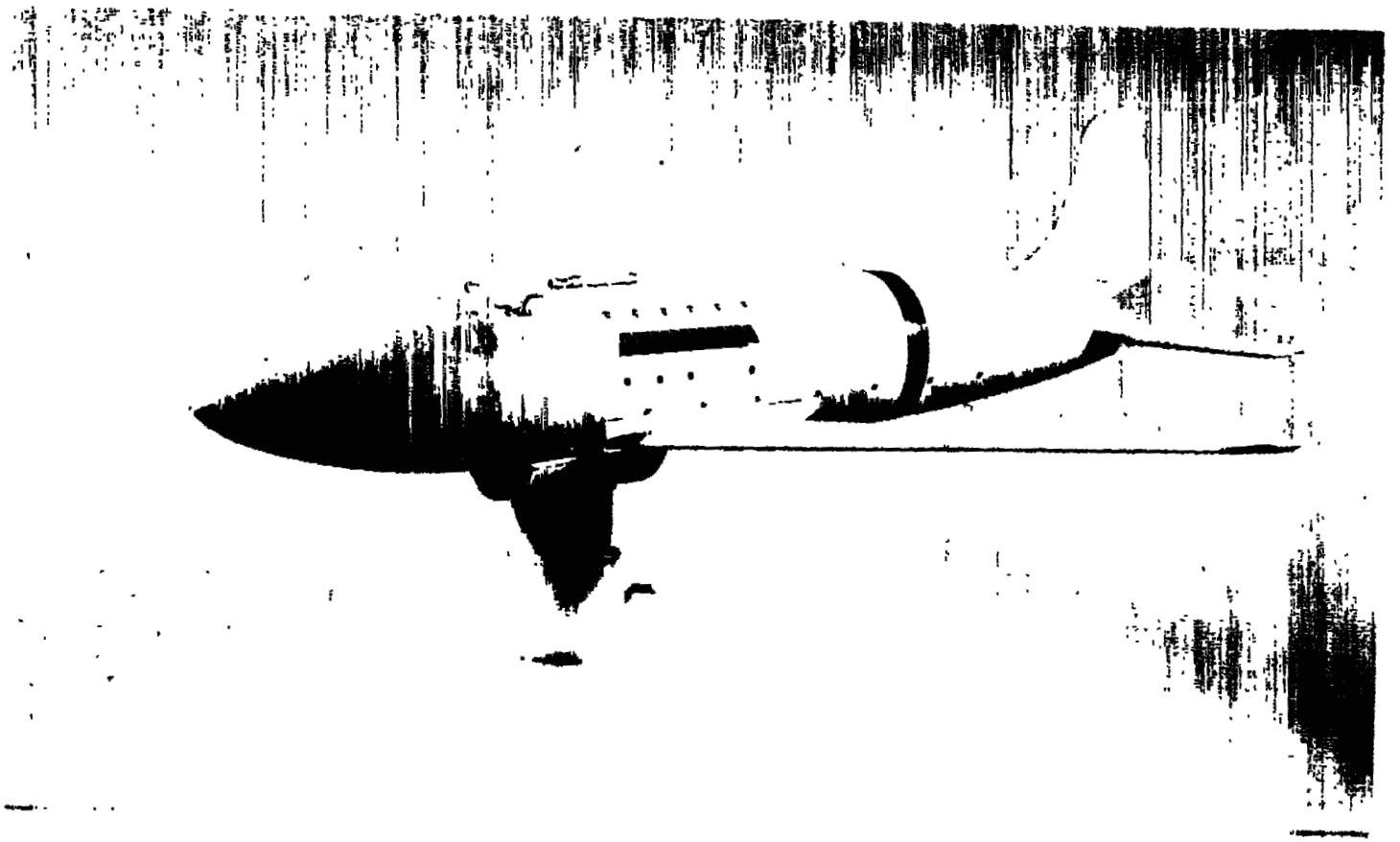

Figure 2.- Photograph of model. L-86304

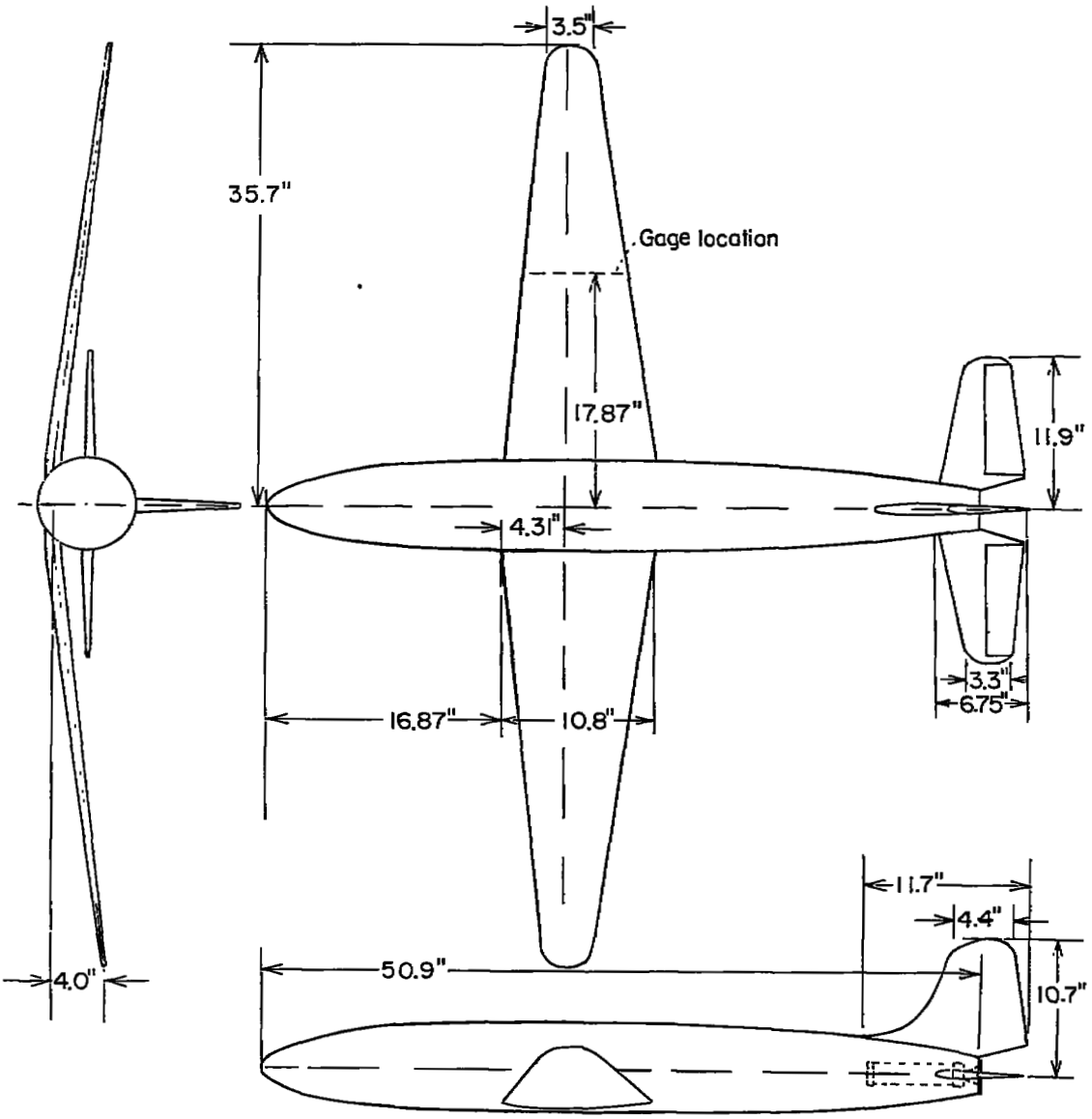

Figure 3.- Three-view drawing of test model.

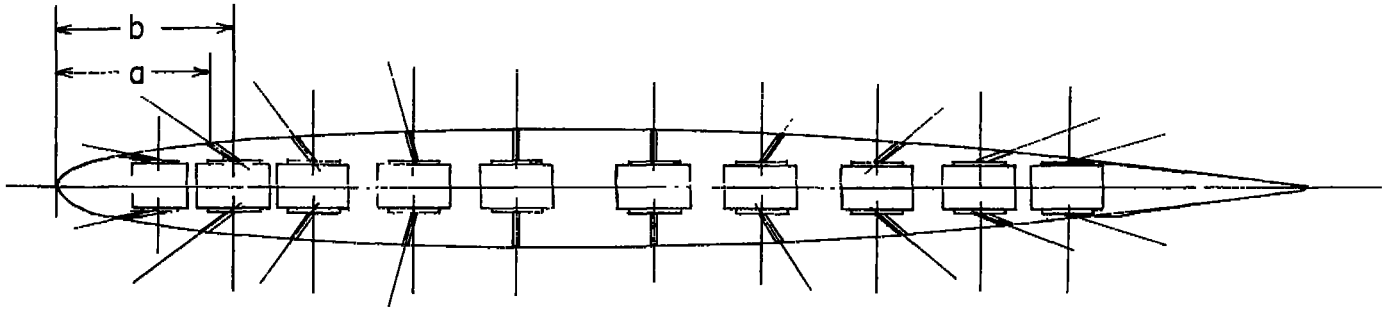

Orifice location, a	Pressure pick-up location, b
.376	.566
.902	1.057
1.428	1.543
2.105	2.145
2.782	2.782
3.609	3.688
4.360	4.260
5.112	4.962
5.789	5.589
6.315	6.115

Figure 4.- Pressure-gage installation in wing.

[redacted]

[redacted]

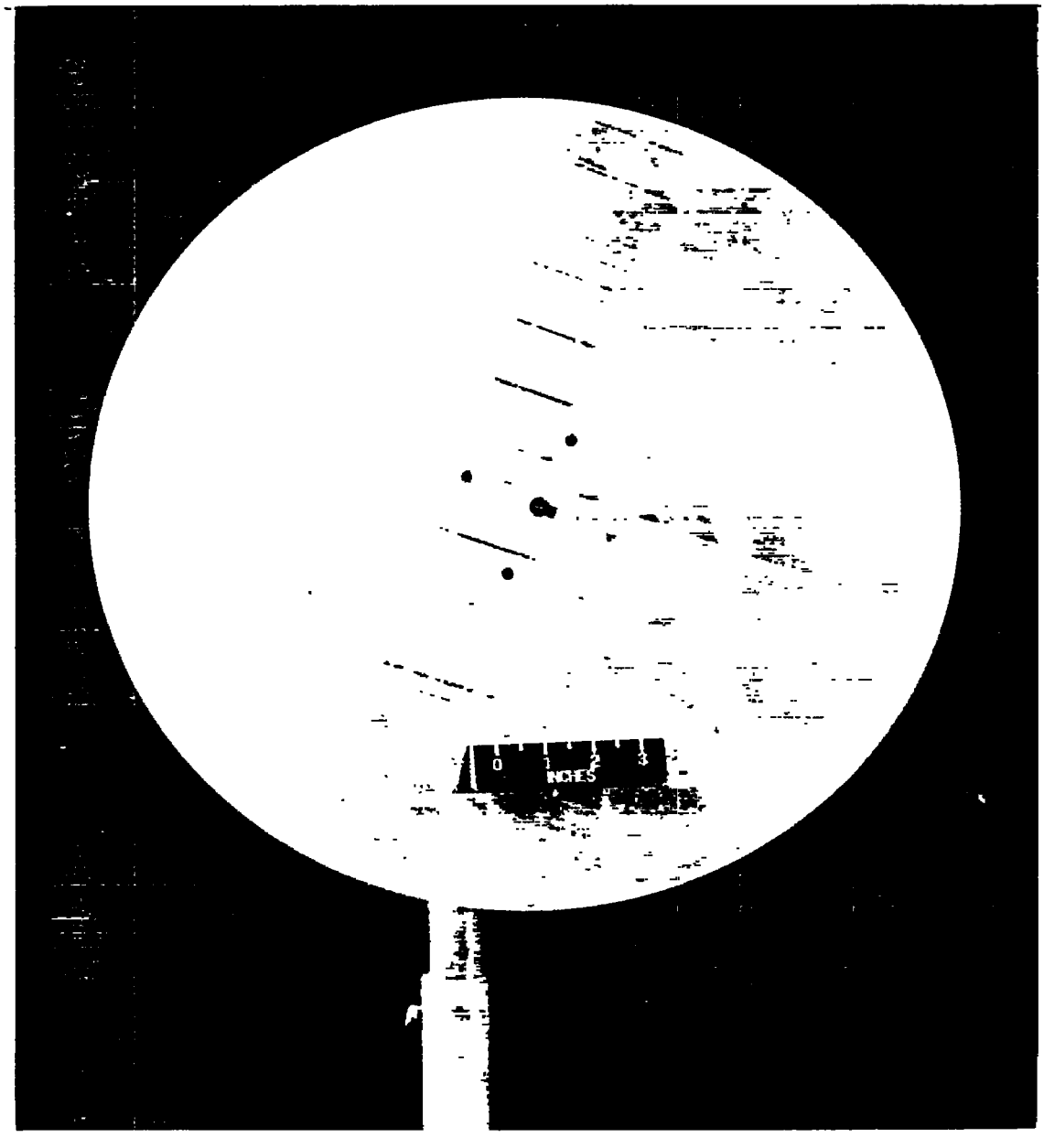

Figure 5.- Photograph of blast gage. L-85041

[redacted]

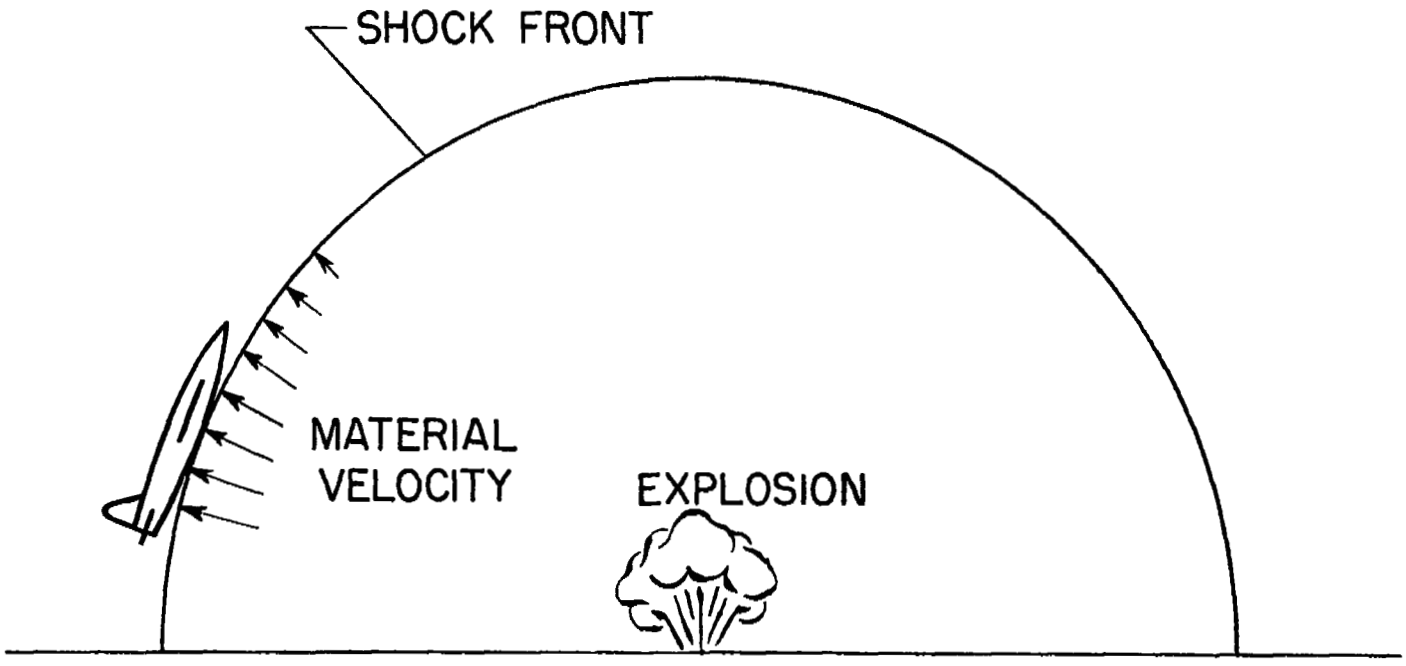

Figure 6.- Conditions at time of shock-front arrival.

[redacted]

[redacted]

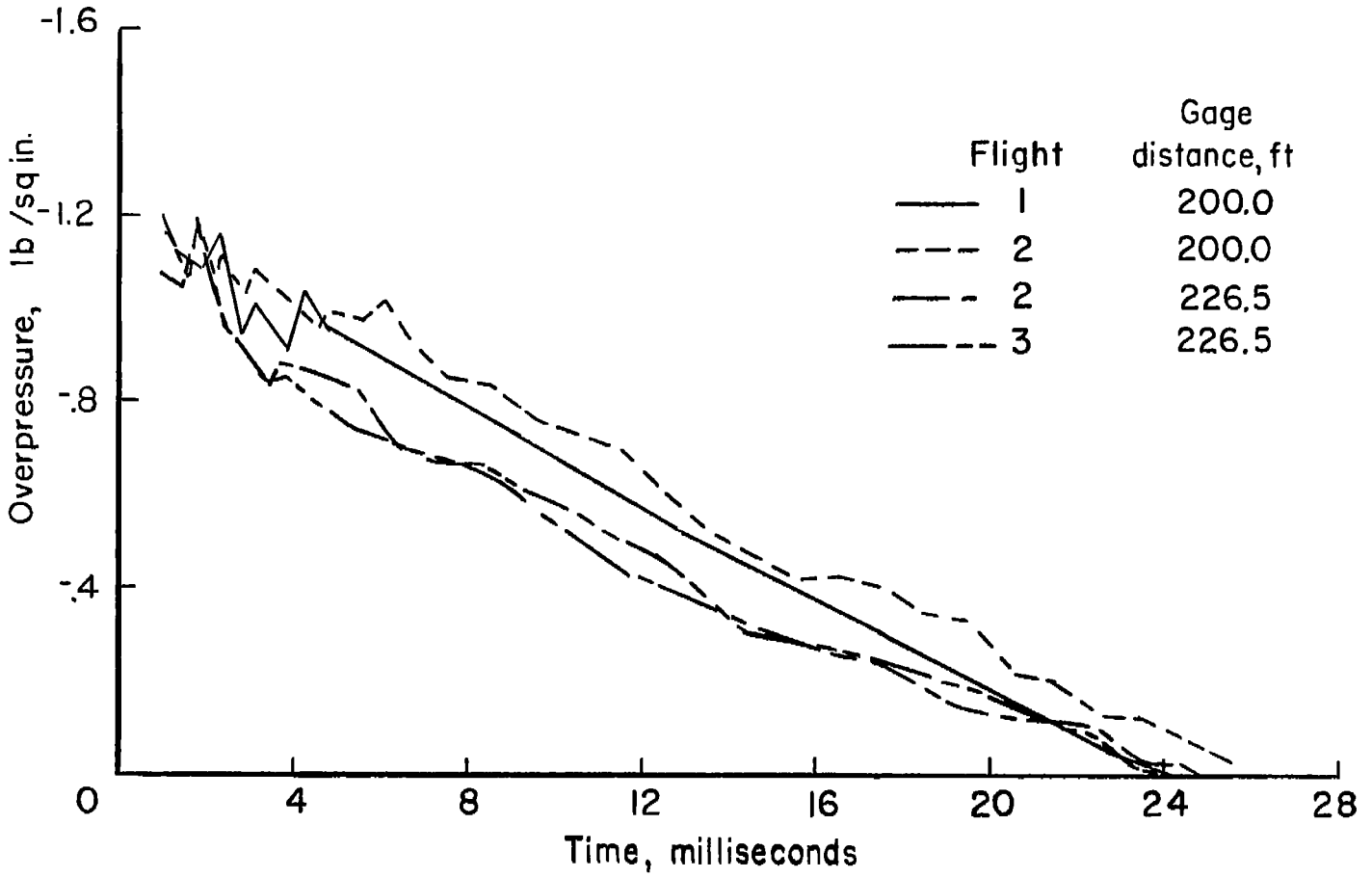

Figure 7.- Time histories of overpressure.

[redacted]

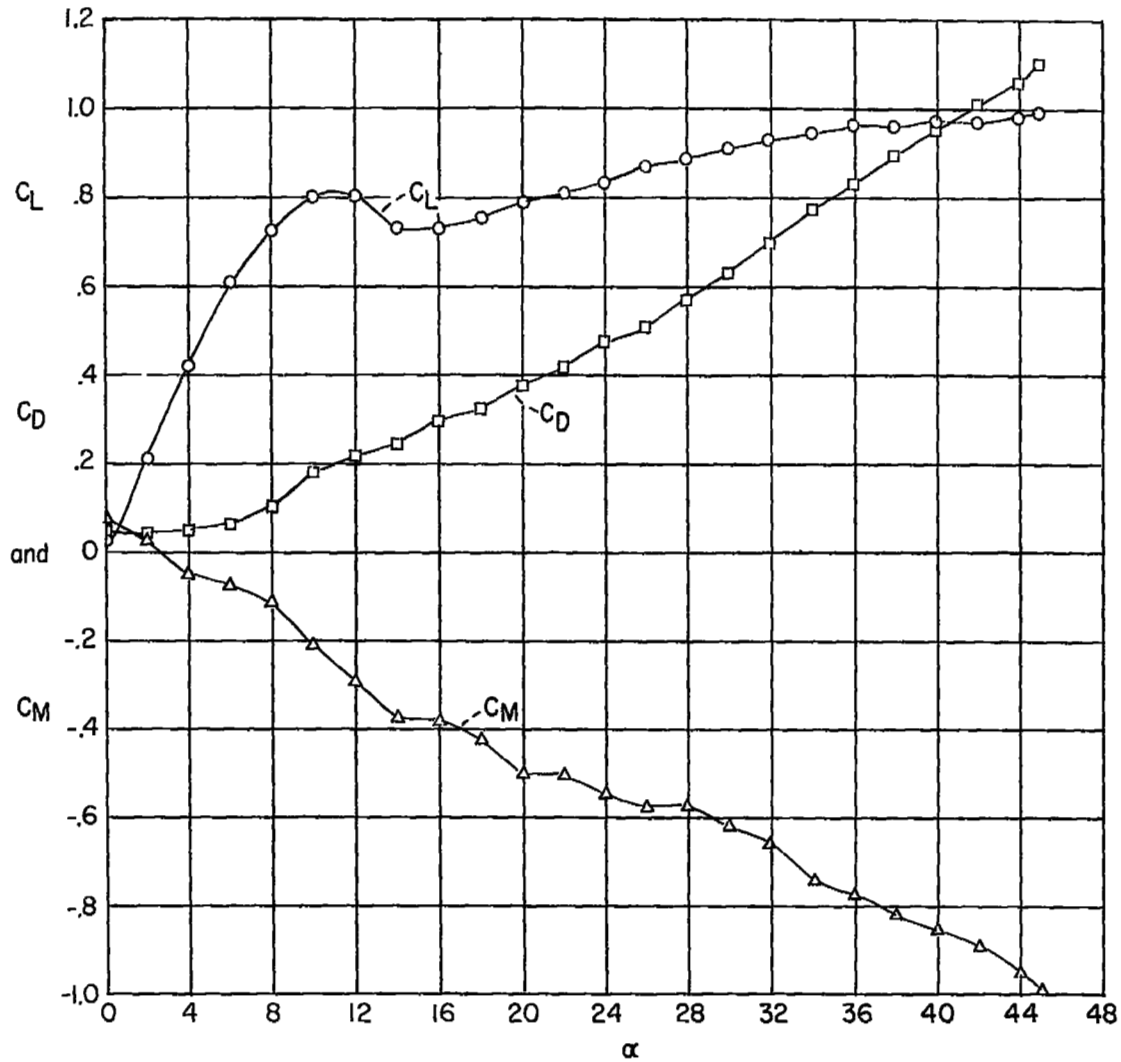

Figure 8.- Results of force tests in wind tunnel.

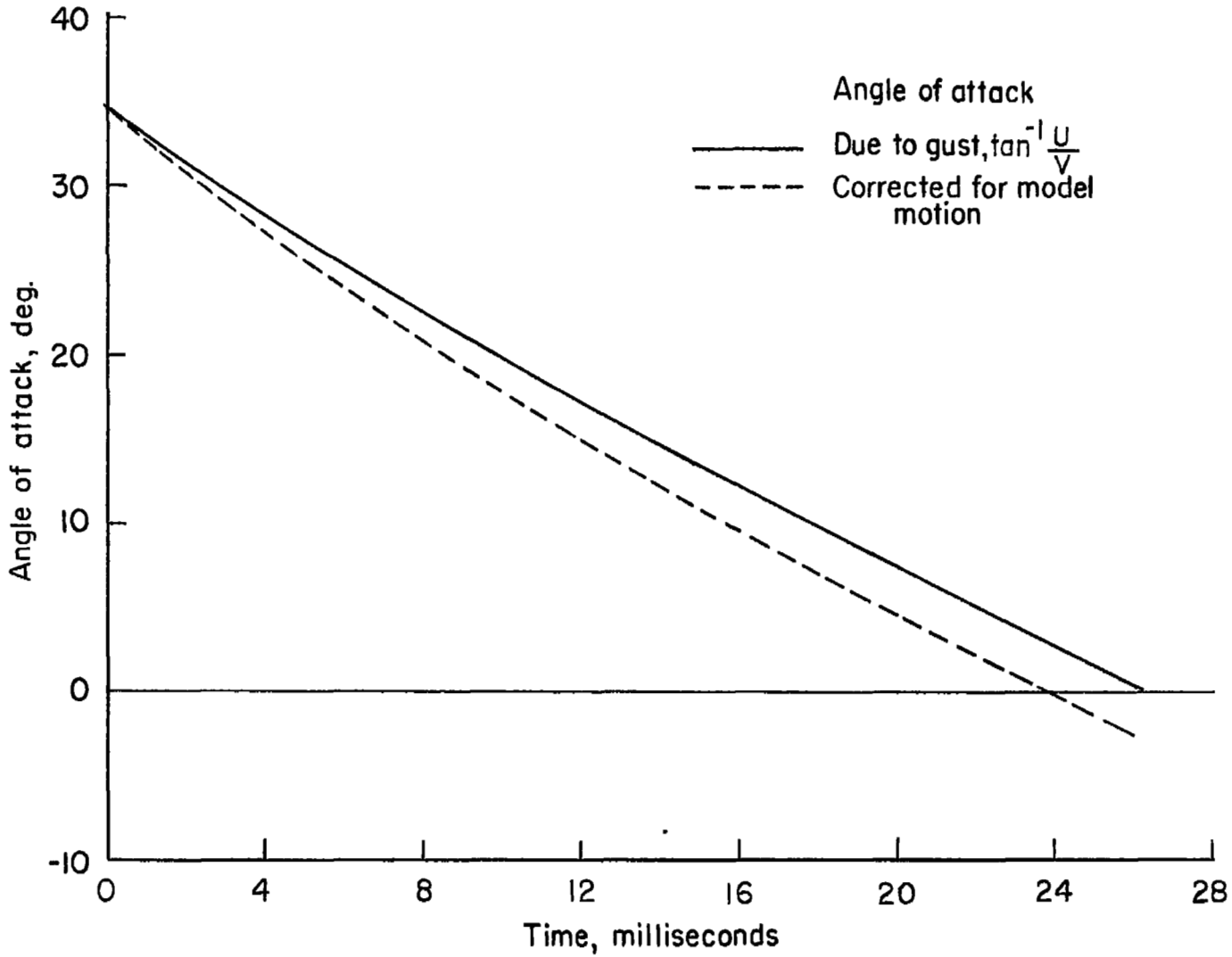

Figure 9.- Angle-of-attack variation.

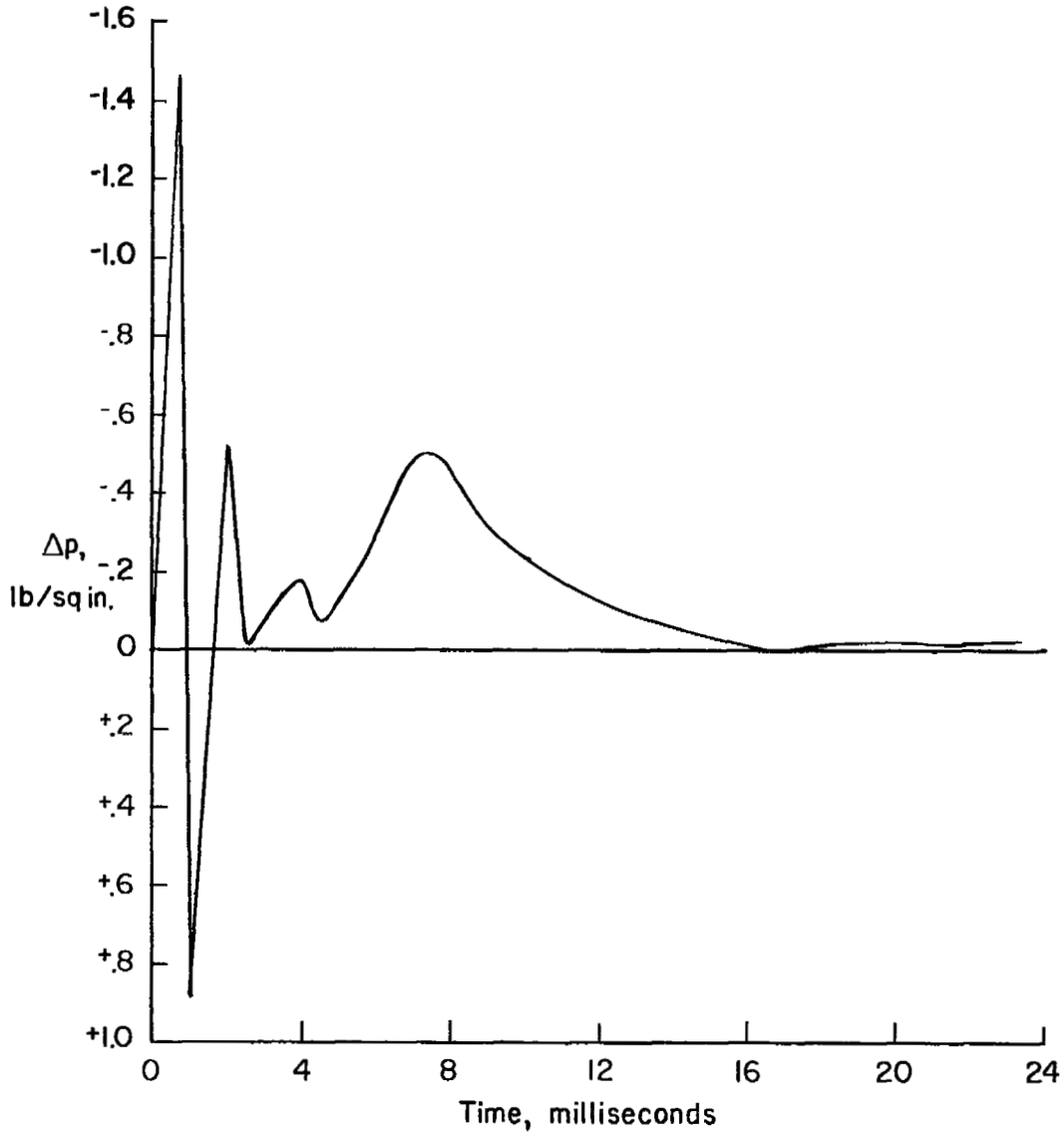

Figure 10.- Sample time history of differential pressure at 37 percent chord.

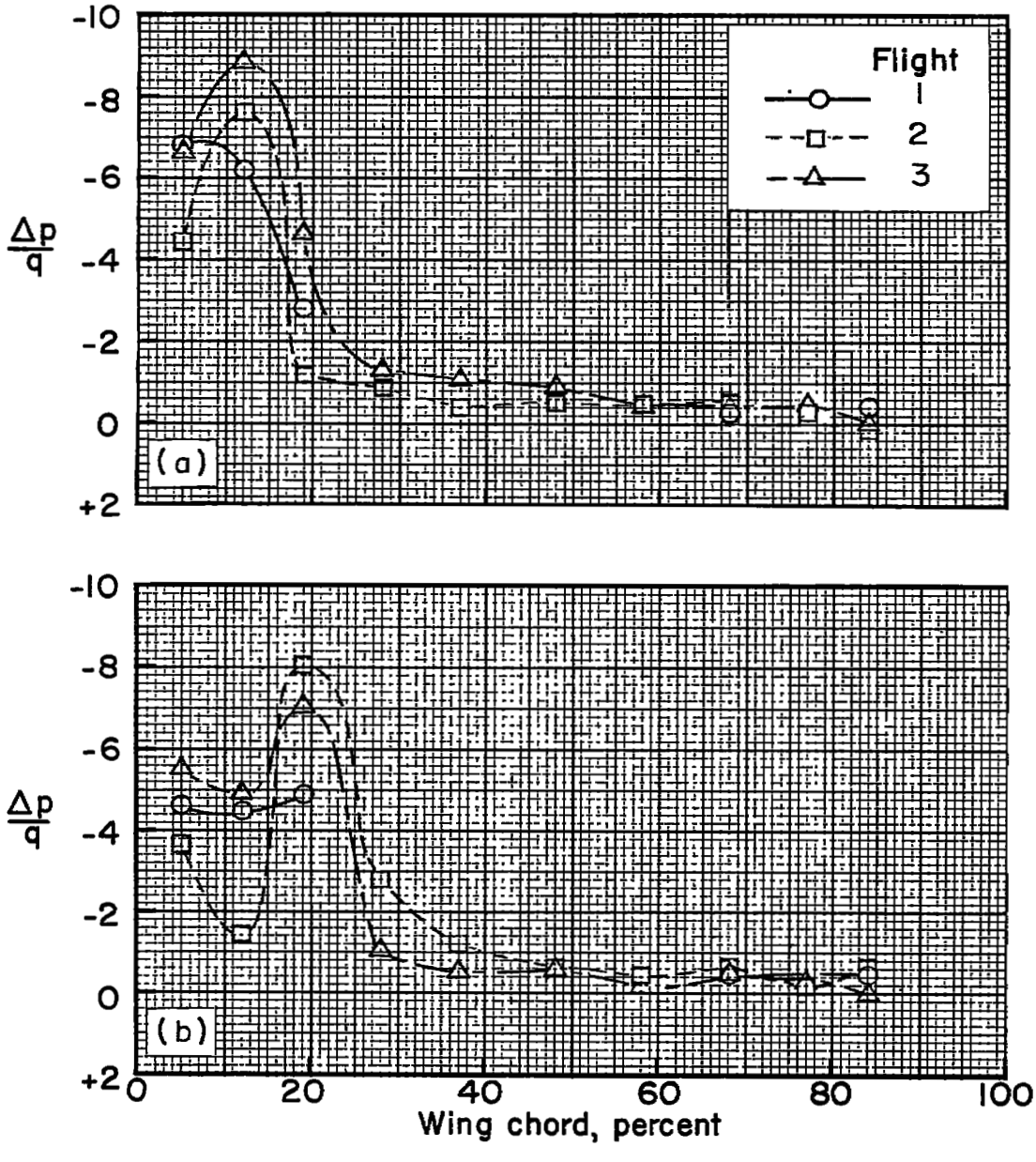

(a) Time, 3 milliseconds; $\alpha = 28.4^{\circ}$; distance, 0.53 chord.

(b) Time, 4 milliseconds; $\alpha = 26.6^{\circ}$; distance, 0.71 chord.

Figure 11.- Chordwise pressure distributions obtained from the three flights.

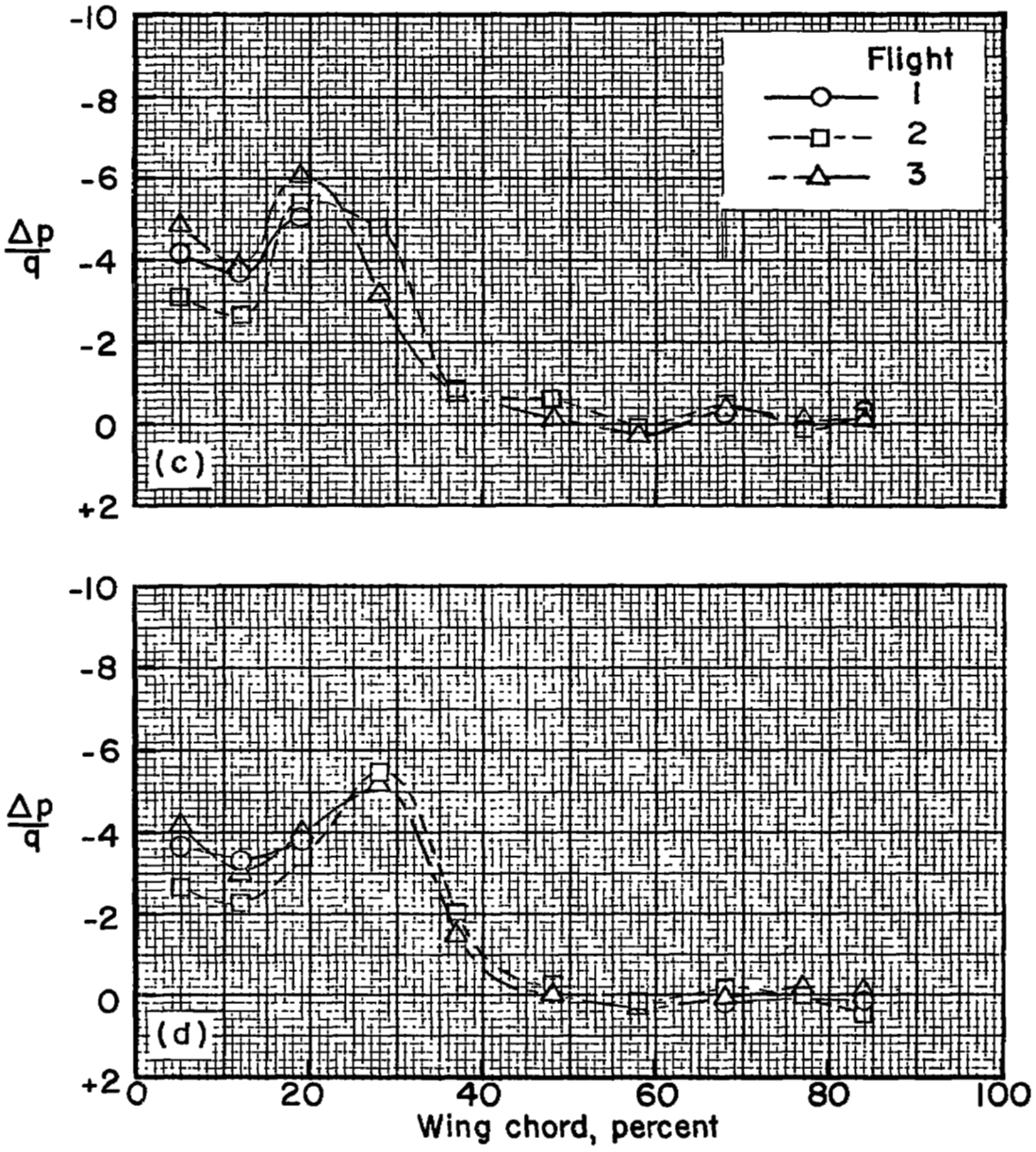

(c) Time, 5 milliseconds; $\alpha = 25.0^{\circ}$; distance, 0.89 chord.

(d) Time, 6 milliseconds; $\alpha = 23.4^{\circ}$; distance, 1.07 chords.

Figure 11.- Continued.

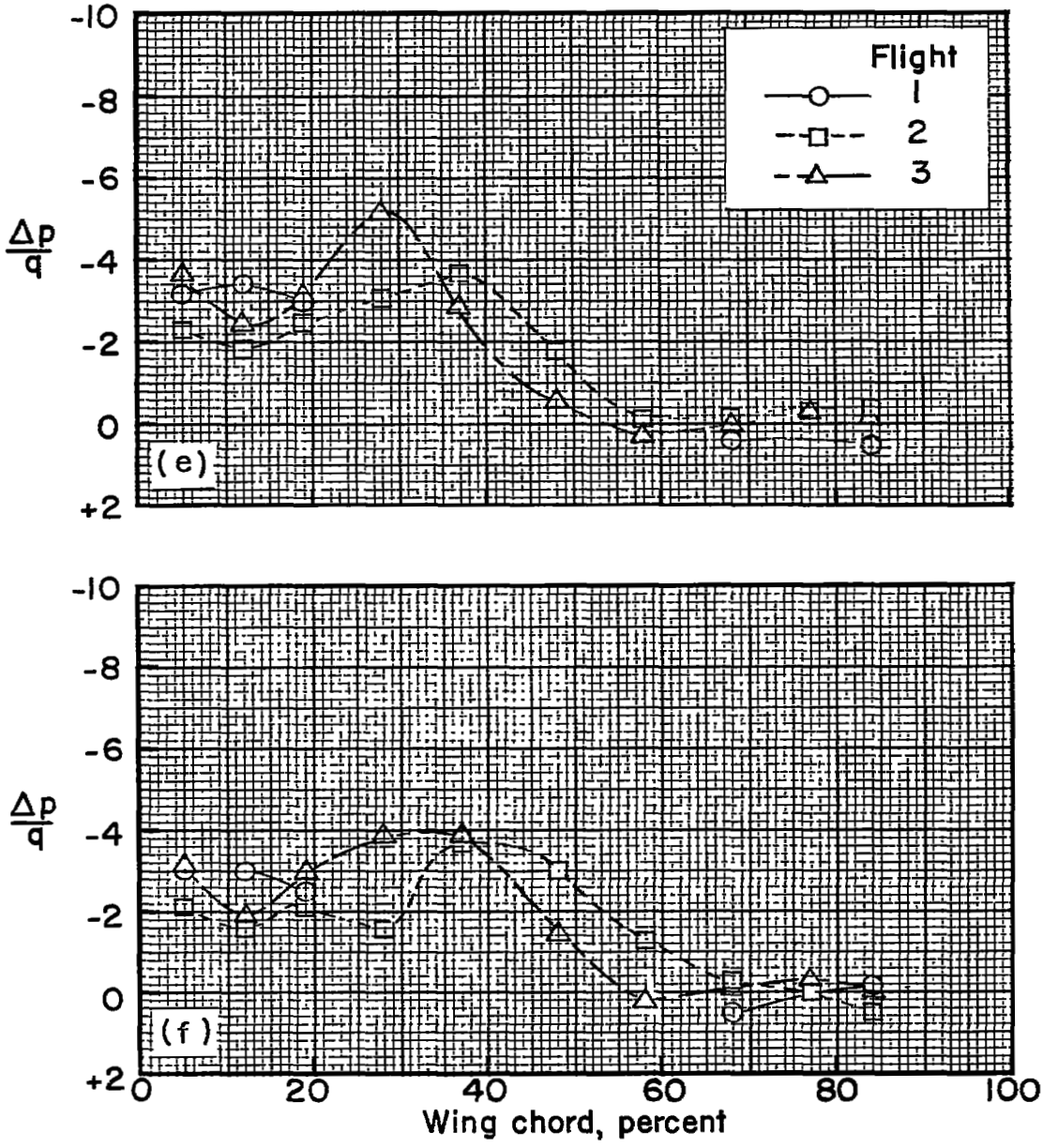

(e) Time, 7 milliseconds; $\alpha = 21.5^{\circ}$; distance, 1.24 chords.

(f) Time, 8 milliseconds; $\alpha = 19.9^{\circ}$; distance, 1.42 chords.

Figure 11.- Continued.

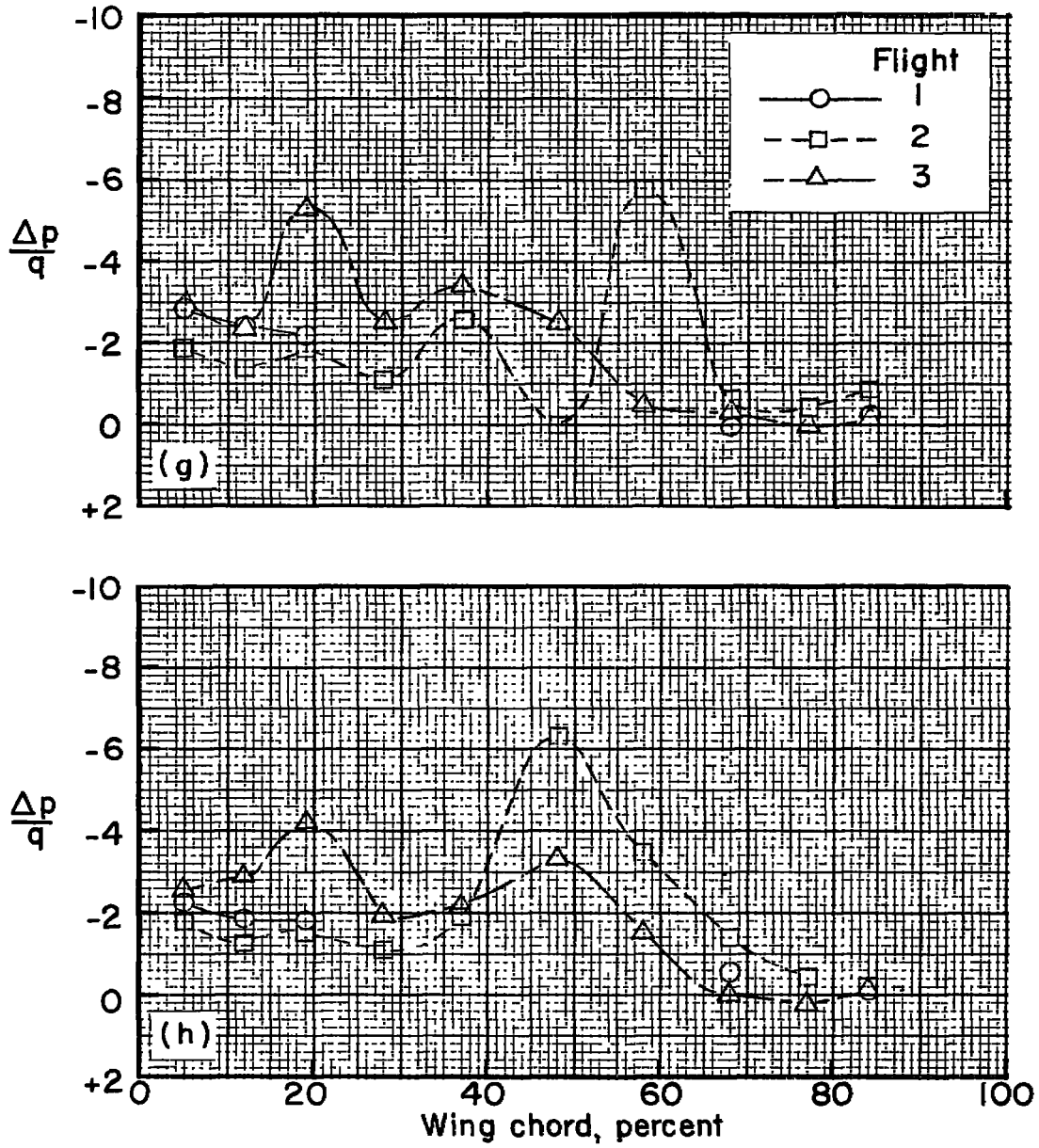

(g) Time, 9 milliseconds; $\alpha = 18.6^{\circ}$; distance, 1.60 chords.

(h) Time, 10 millisecords; $\alpha = 16.9^{\circ}$; distance, 1.78 chords.

Figure 11.- Continued.

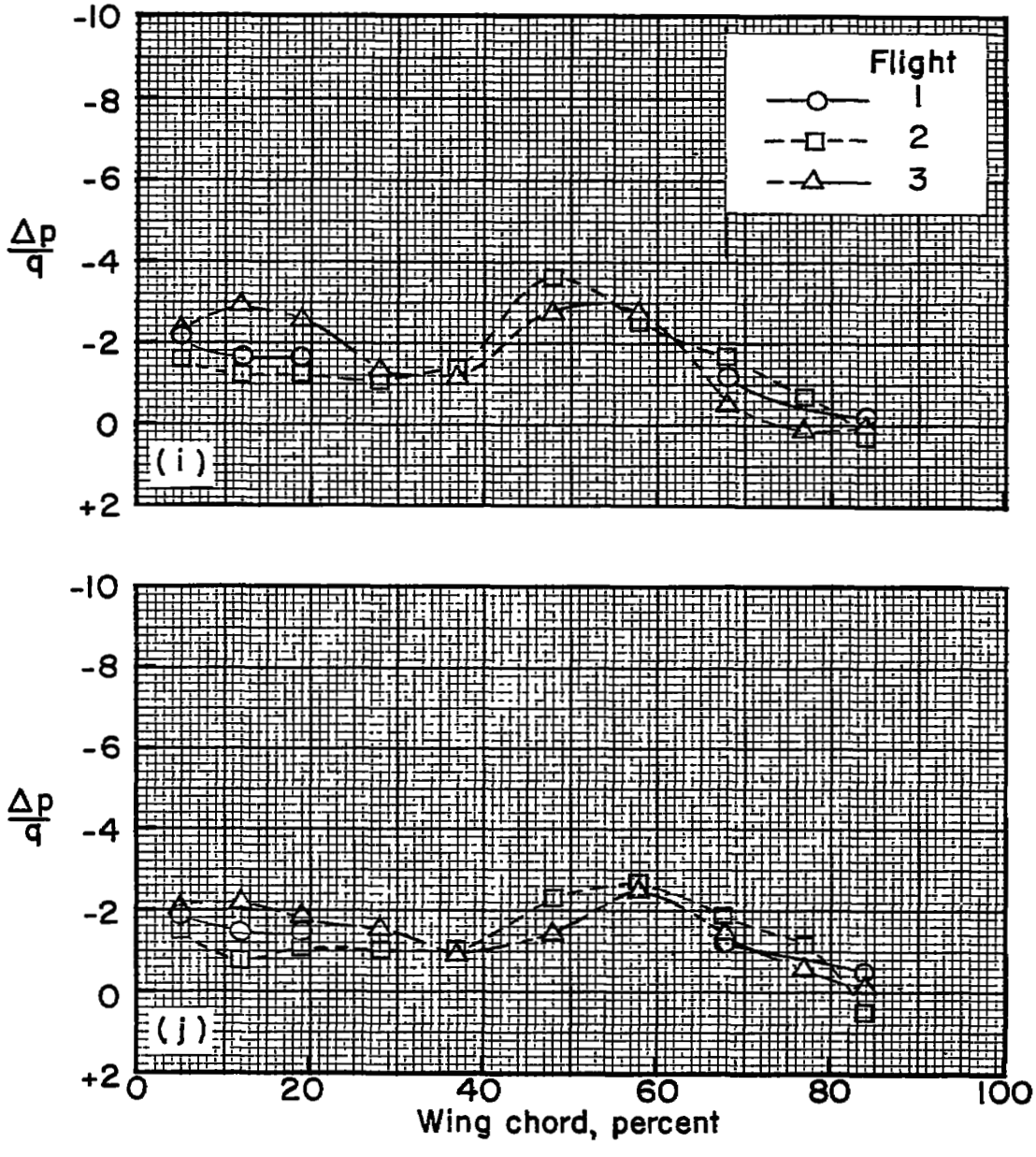

(i) Time, 11 milliseconds; $\alpha = 15.4^{\circ}$; distance, 1.96 chords.

(j) Time, 12 milliseconds; $\alpha = 13.8^{\circ}$; distance, 2.13 chords.

Figure 11.- Continued.

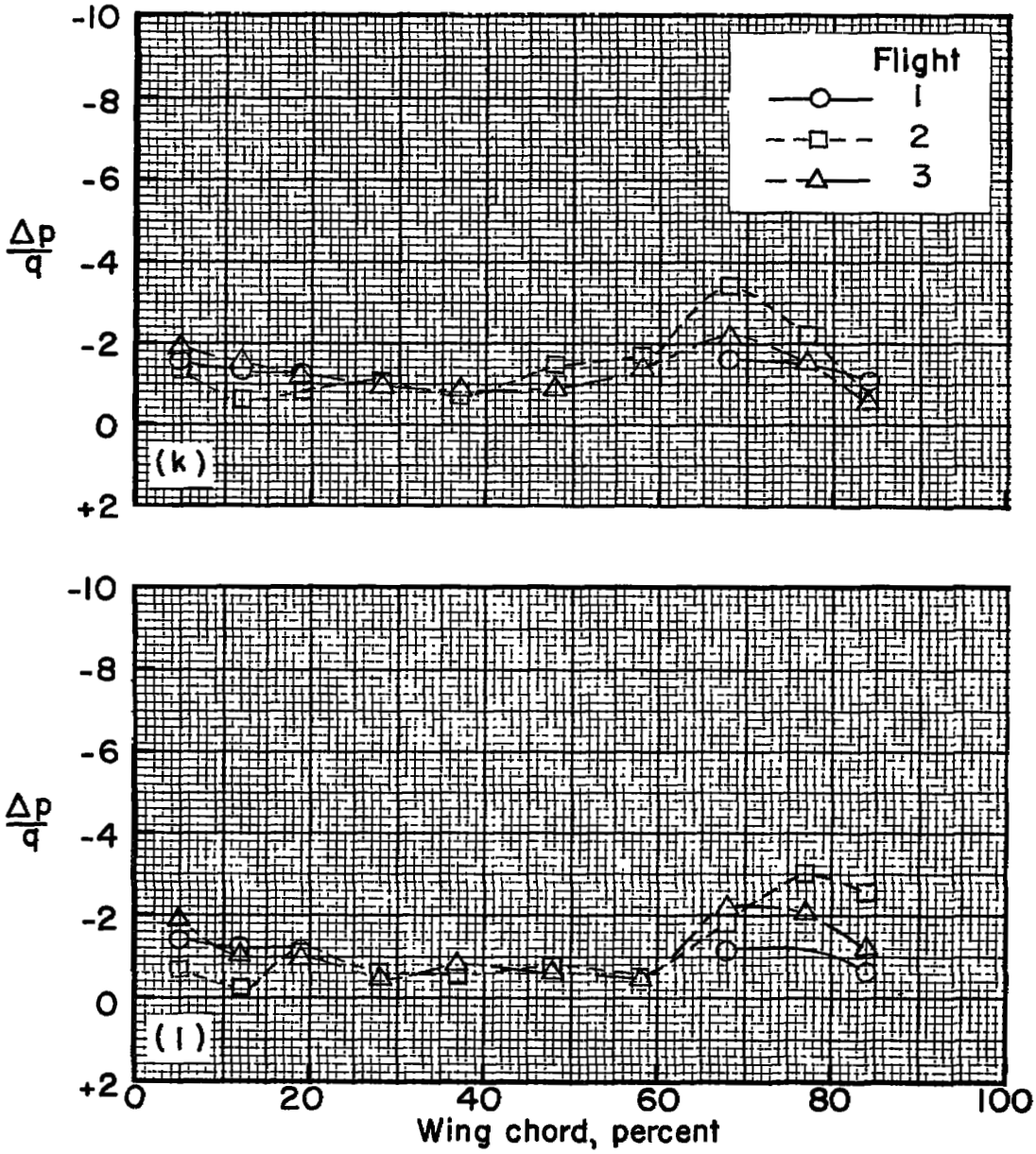

(k) Time, 13 milliseconds; $\alpha = 12.5^{\circ}$; distance, 2.31 chords.

(l) Time, 14 milliseconds; $\alpha = 11.0^{\circ}$; distance, 2.49 chords.

Figure 11.- Continued.

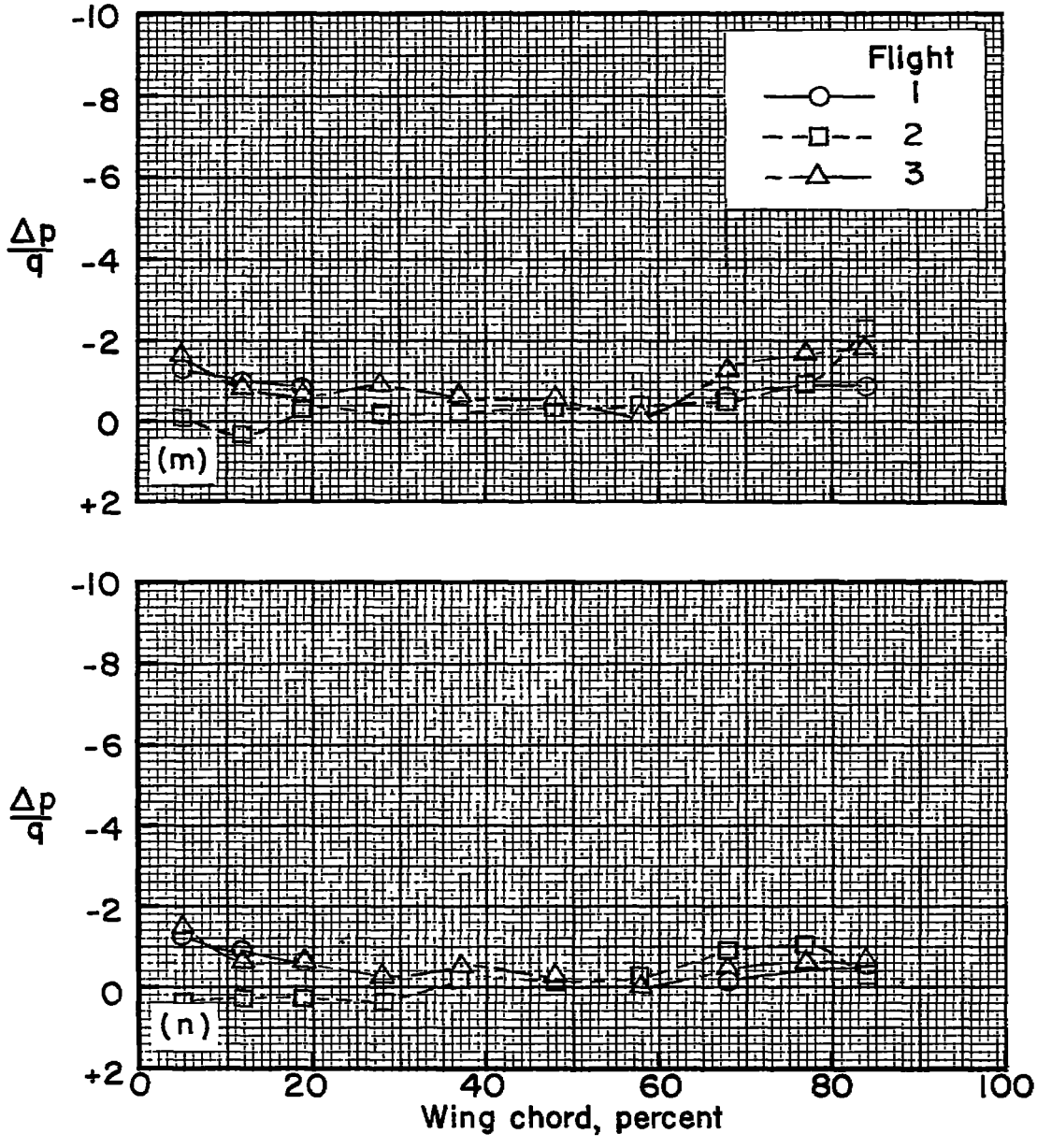

(m) Time, 15 milliseconds; $\alpha = 9.7^{\circ}$; distance, 2.67 chords.

(n) Time, 16 milliseconds; $\alpha = 8.5^{\circ}$; distance, 2.84 chords.

Figure 11.- Continued.

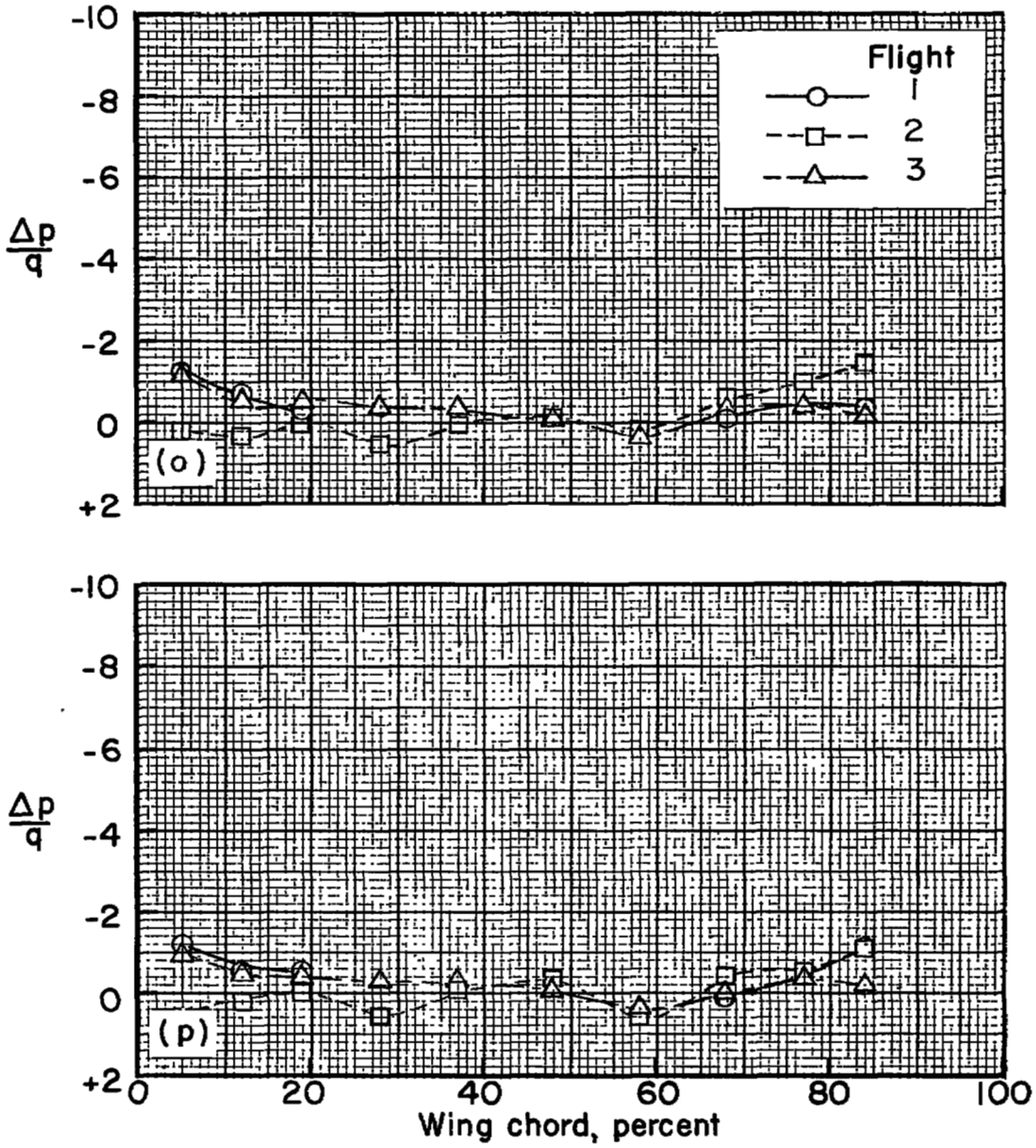

(o) Time, 17 milliseconds; $\alpha = 7.2^{\circ}$; distance, 3.02 chords.

(p) Time, 18 milliseconds; $\alpha = 6.2^{\circ}$; distance, 3.20 chords.

Figure 11.- Continued.

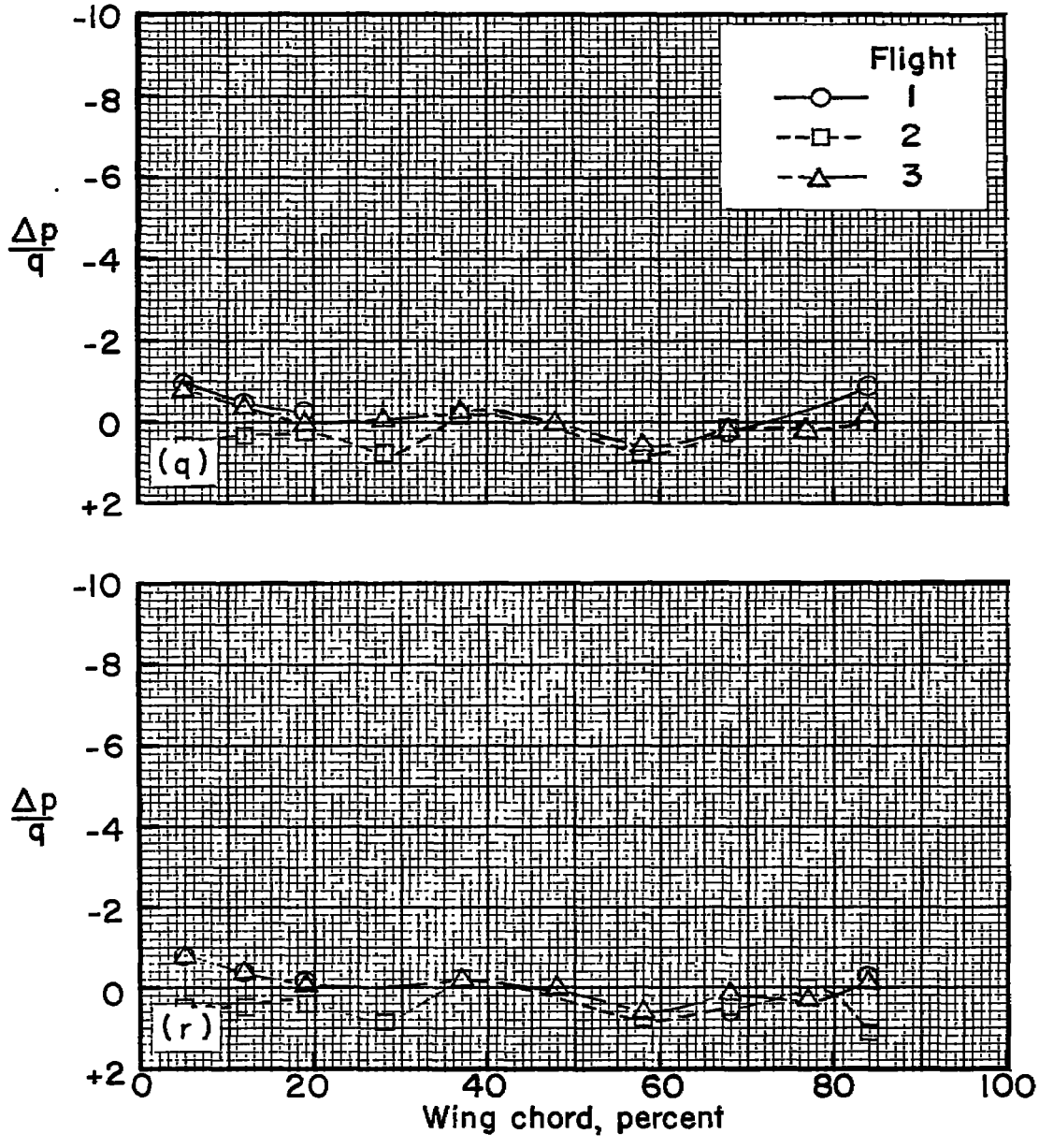

(q) Time, 19 milliseconds; $\alpha = 4.8^{\circ}$; distance, 3.38 chords.

(r) Time, 20 milliseconds; $\alpha = 3.8^{\circ}$; distance, 3.56 chords.

Figure 11.- Concluded.

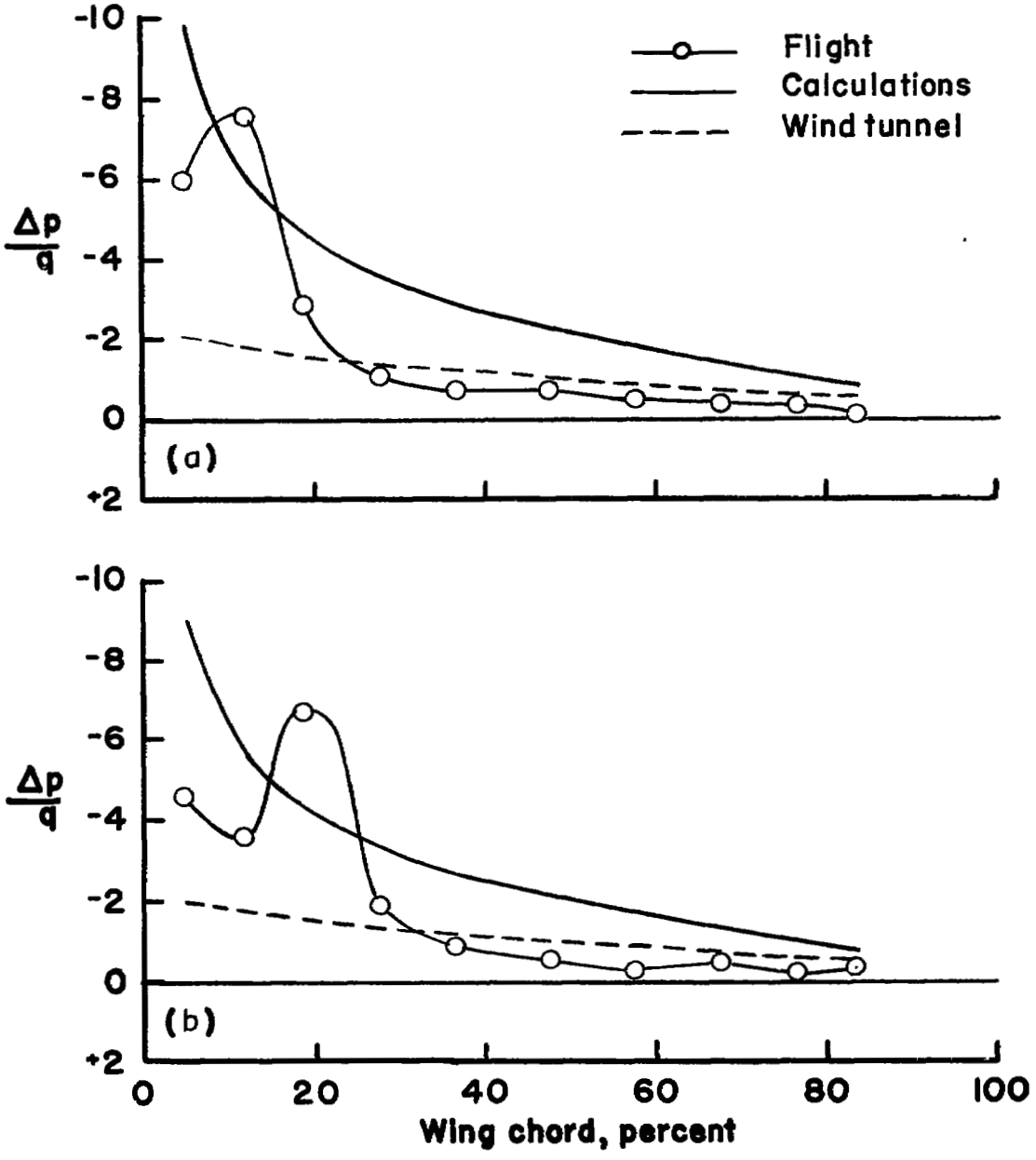

(a) Time, 3 milliseconds; $\alpha = 28.4^{\circ}$; distance, 0.53 chord.

(b) Time, 4 milliseconds; $\alpha = 26.6^{\circ}$; distance, 0.71 chord.

Figure 12.- Comparison of chordwise pressure distributions obtained from flights, calculations, and wind-tunnel tests.

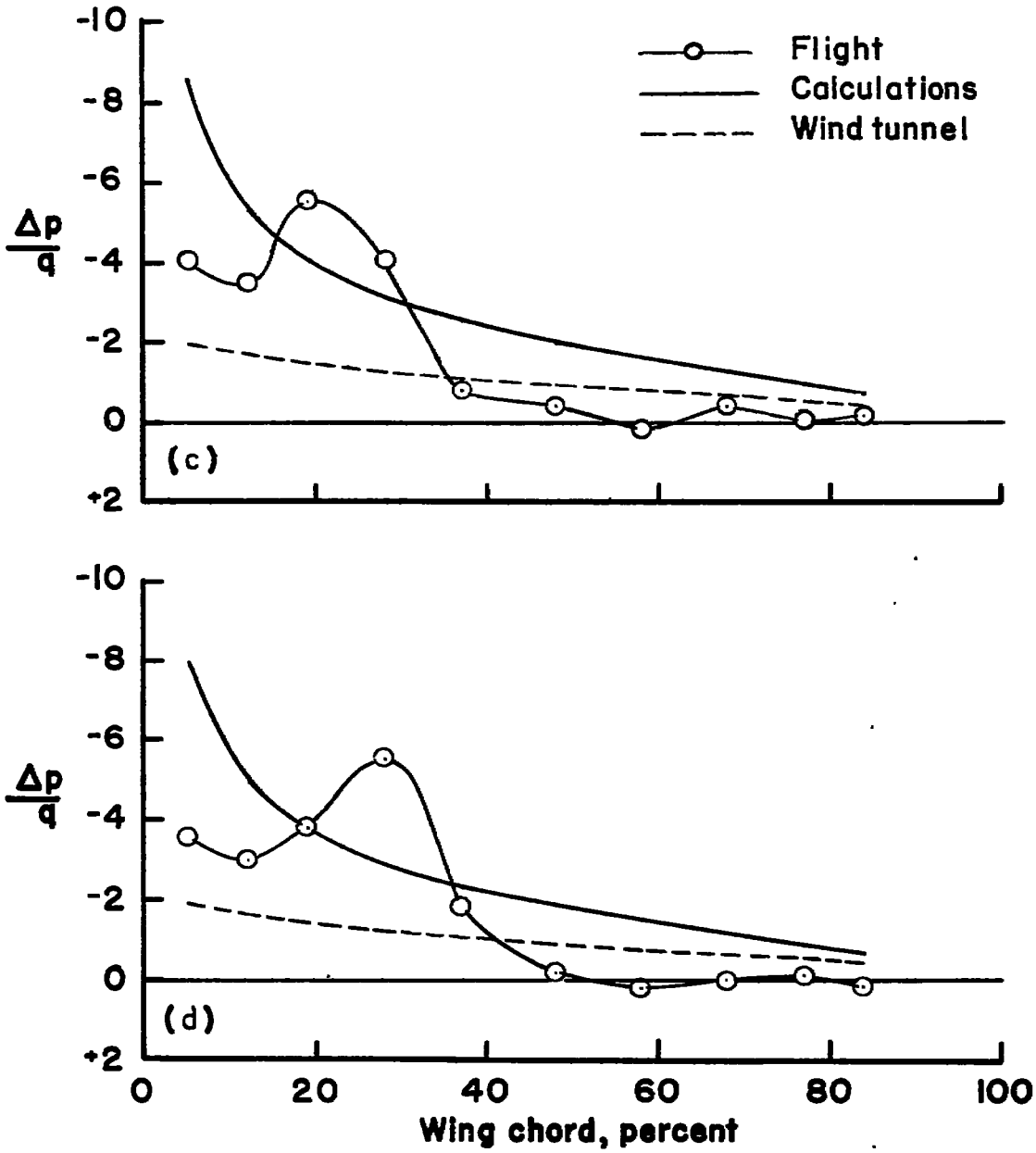

(c) Time, 5 milliseconds; $\alpha = 25.0^{\circ}$; distance, 0.89 chord.

(d) Time, 6 milliseconds; $\alpha = 23.4^{\circ}$; distance, 1.07 chords.

Figure 12.- Continued.

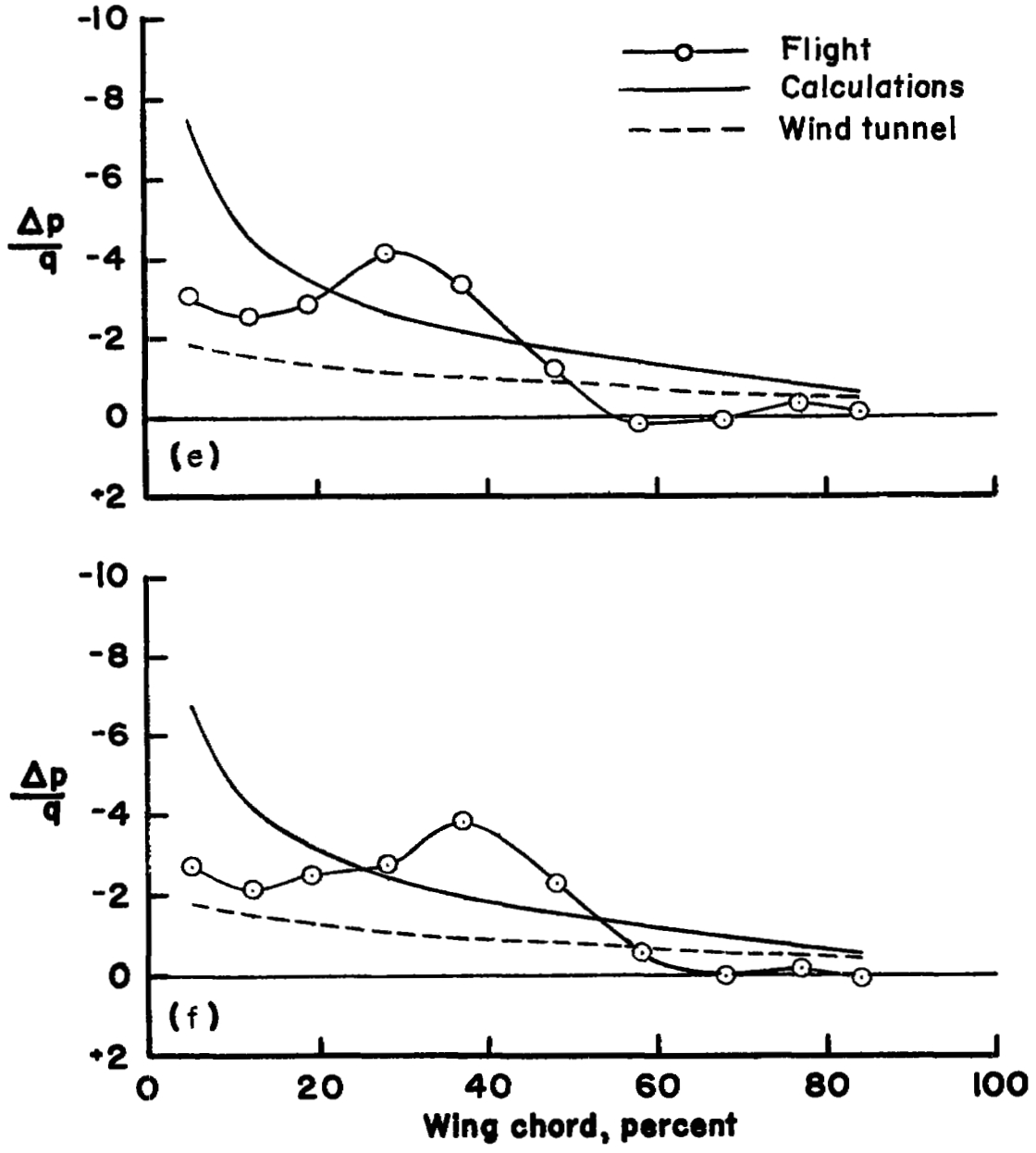

(e) Time, 7 milliseconds; $\alpha = 21.5^{\circ}$; distance, 1.24 chords.

(f) Time, 8 milliseconds; $\alpha = 19.9^{\circ}$; distance, 1.42 chords.

Figure 12.- Continued.

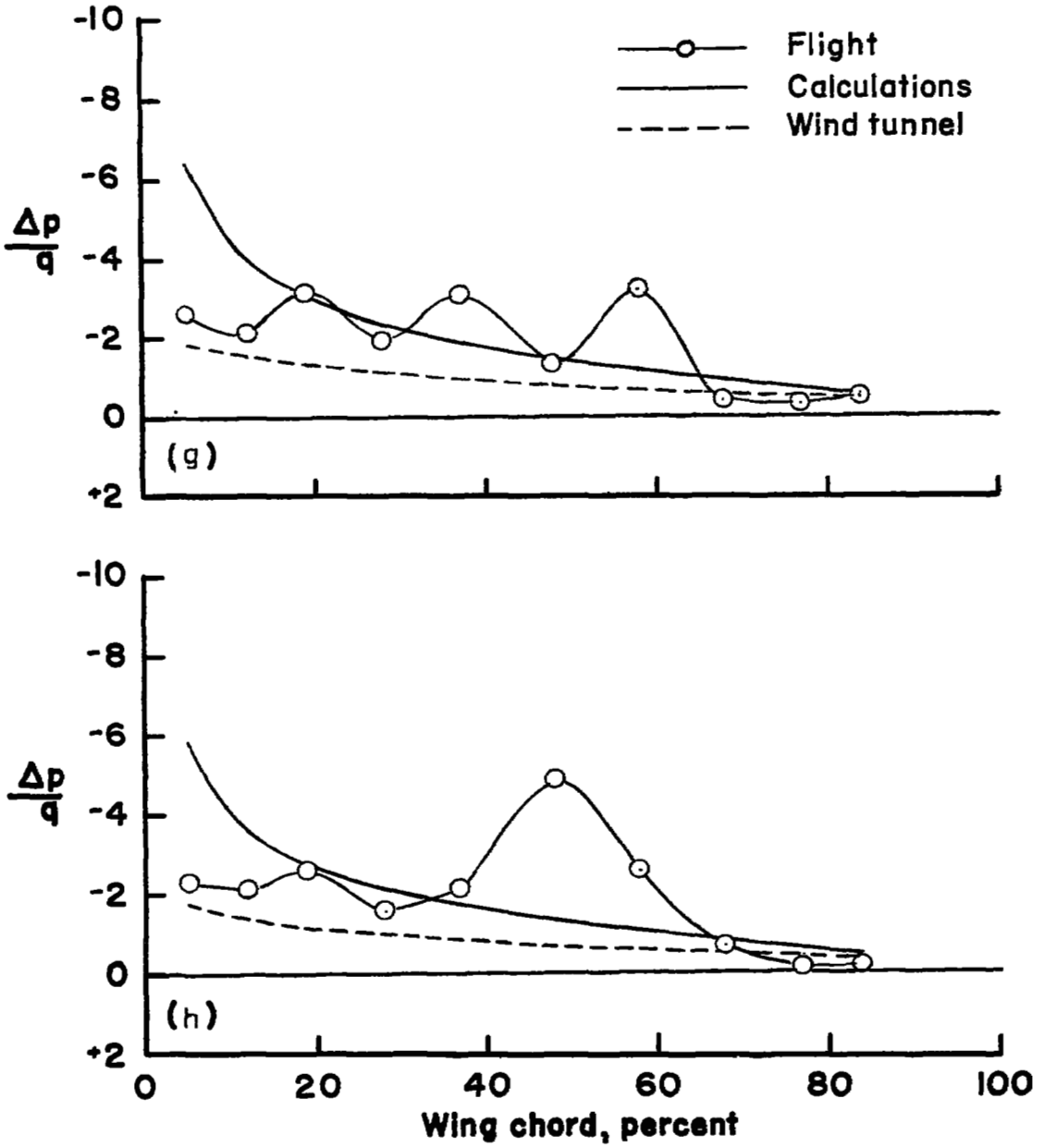

(g) Time, 9 milliseconds; $\alpha = 18.6^{\circ}$; distance, 1.60 chords.

(h) Time, 10 milliseconds; $\alpha = 16.9^{\circ}$; distance, 1.78 chords.

Figure 12.- Continued.

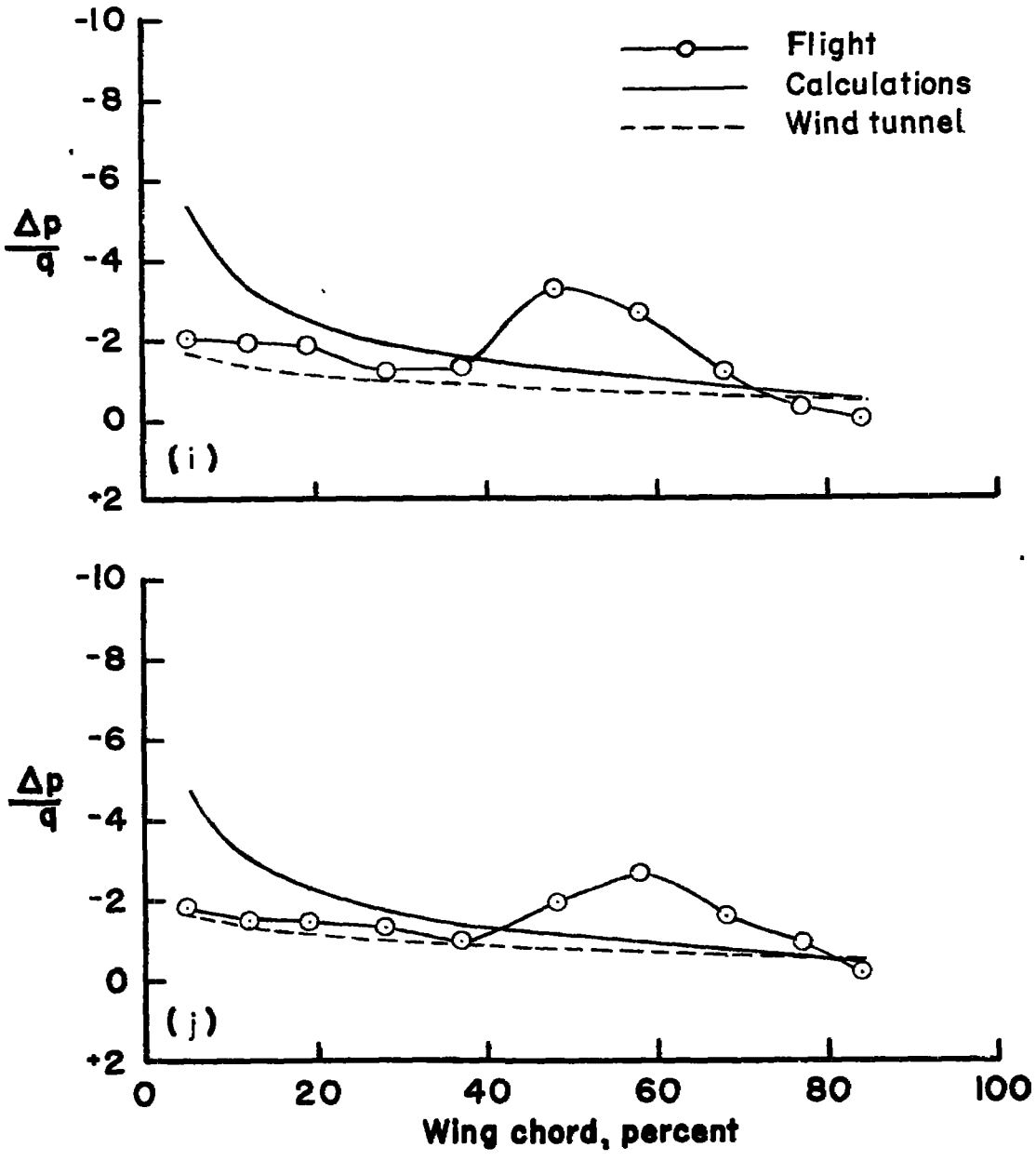

(i) Time, 11 milliseconds; $\alpha = 15.4^{\circ}$; distance, 1.96 chords.

(j) Time, 12 milliseconds; $\alpha = 13.8^{\circ}$; distance; 2.13 chords.

Figure 12.- Continued.

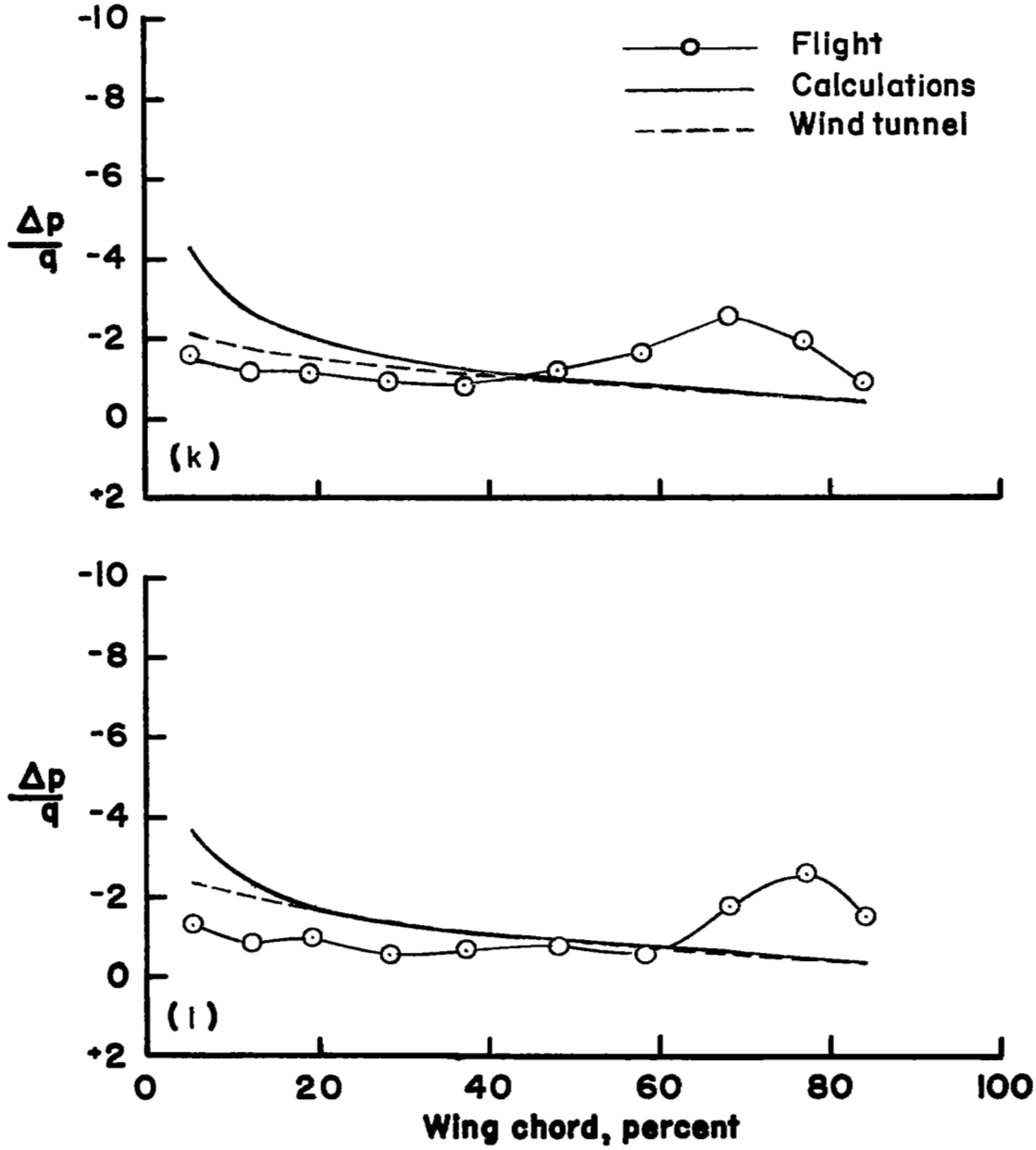

(k) Time, 13 milliseconds; $\alpha = 12.5^{\circ}$; distance, 2.31 chords.

(l) Time, 14 milliseconds; $\alpha = 11.0^{\circ}$; distance, 2.49 chords.

Figure 12.- Continued.

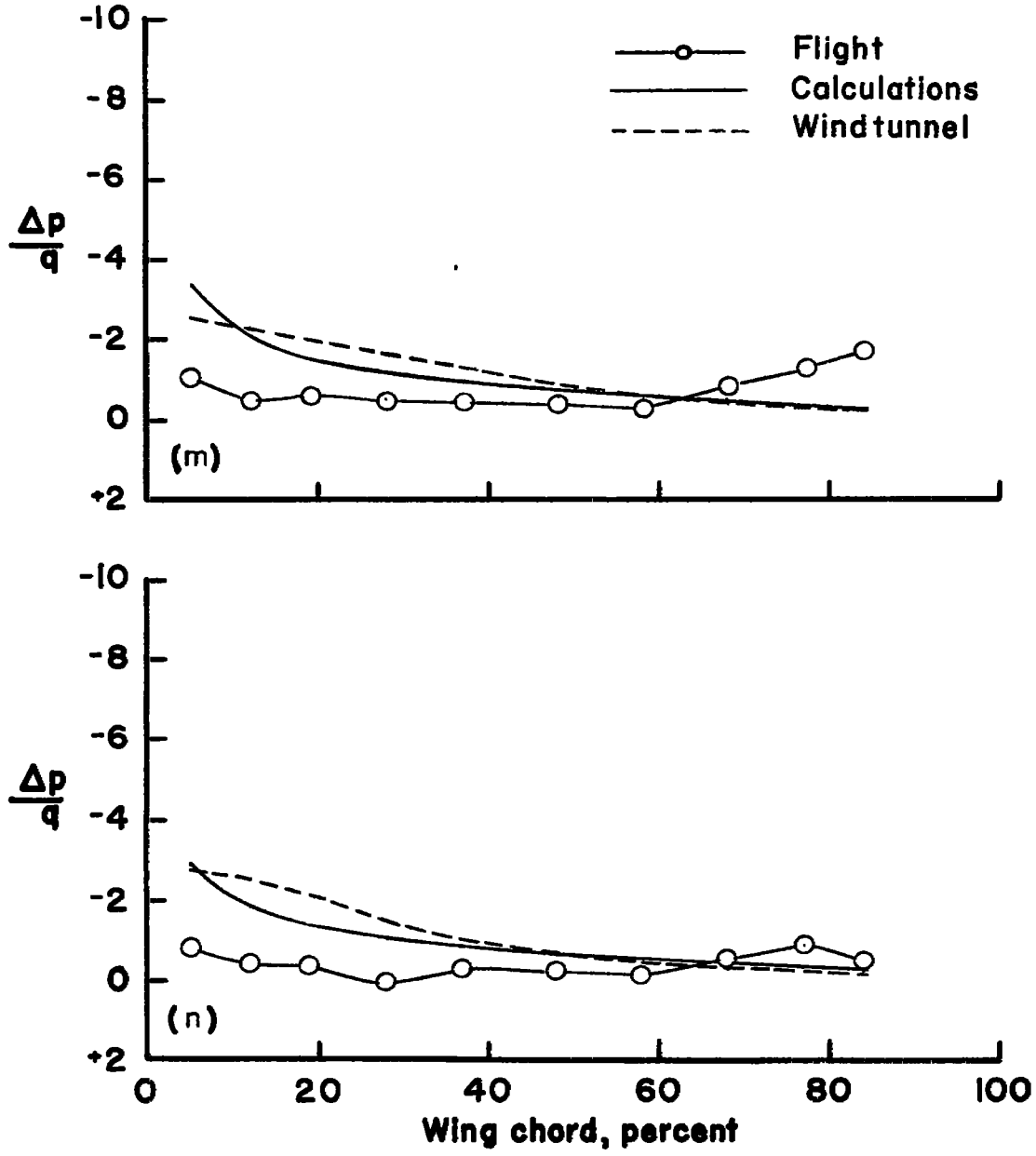

(m) Time, 15 milliseconds; $\alpha = 9.7^{\circ}$; distance, 2.67 chords.

(n) Time, 16 milliseconds; $\alpha = 8.5^{\circ}$; distance, 2.84 chords.

Figure 12.- Continued.

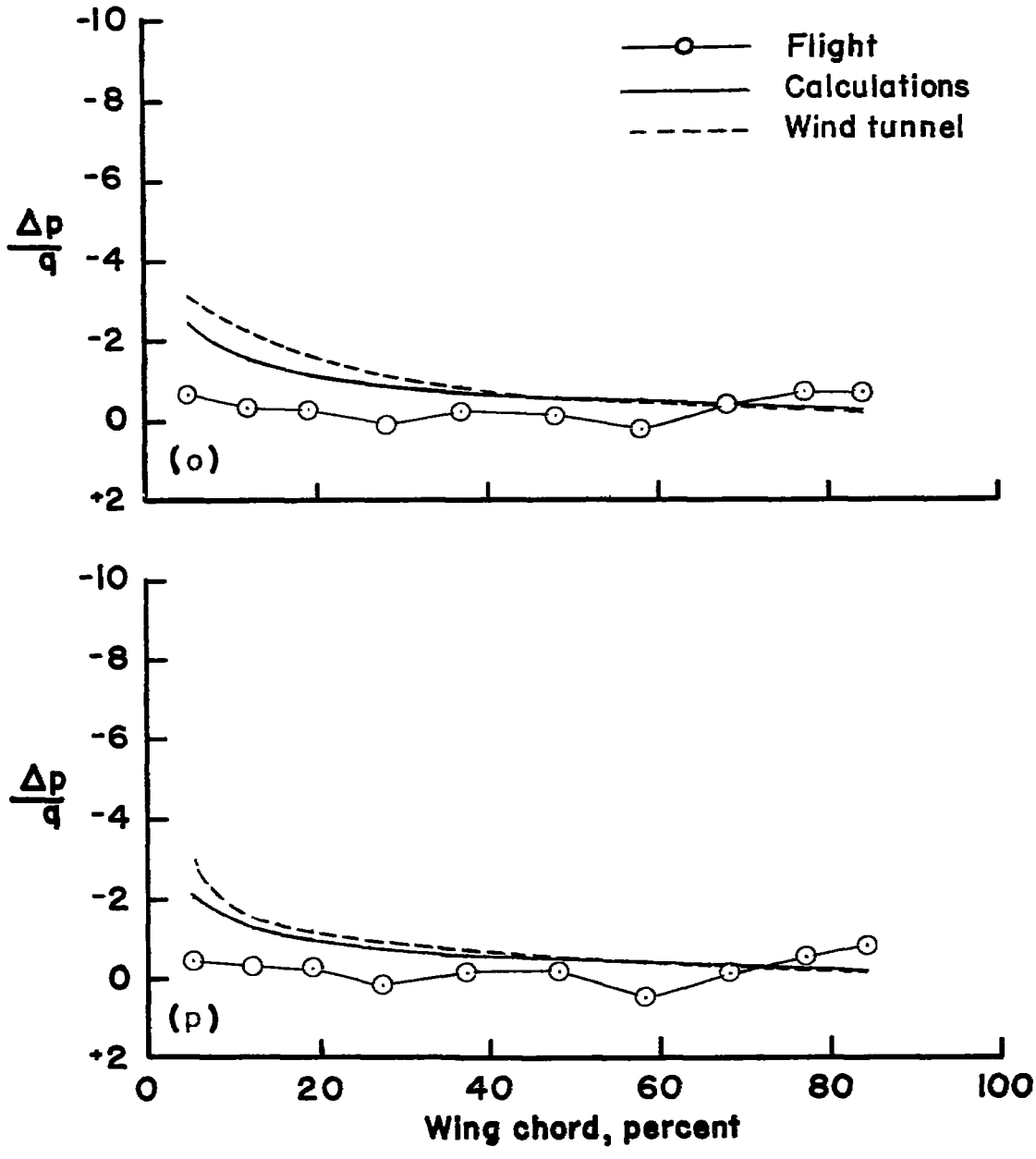

(o) Time, 17 milliseconds; $\alpha = 7.2^{\circ}$; distance, 3.02 chords.

(p) Time, 18 milliseconds; $\alpha = 6.2^{\circ}$; distance, 3.20 chords.

Figure 12.- Continued.

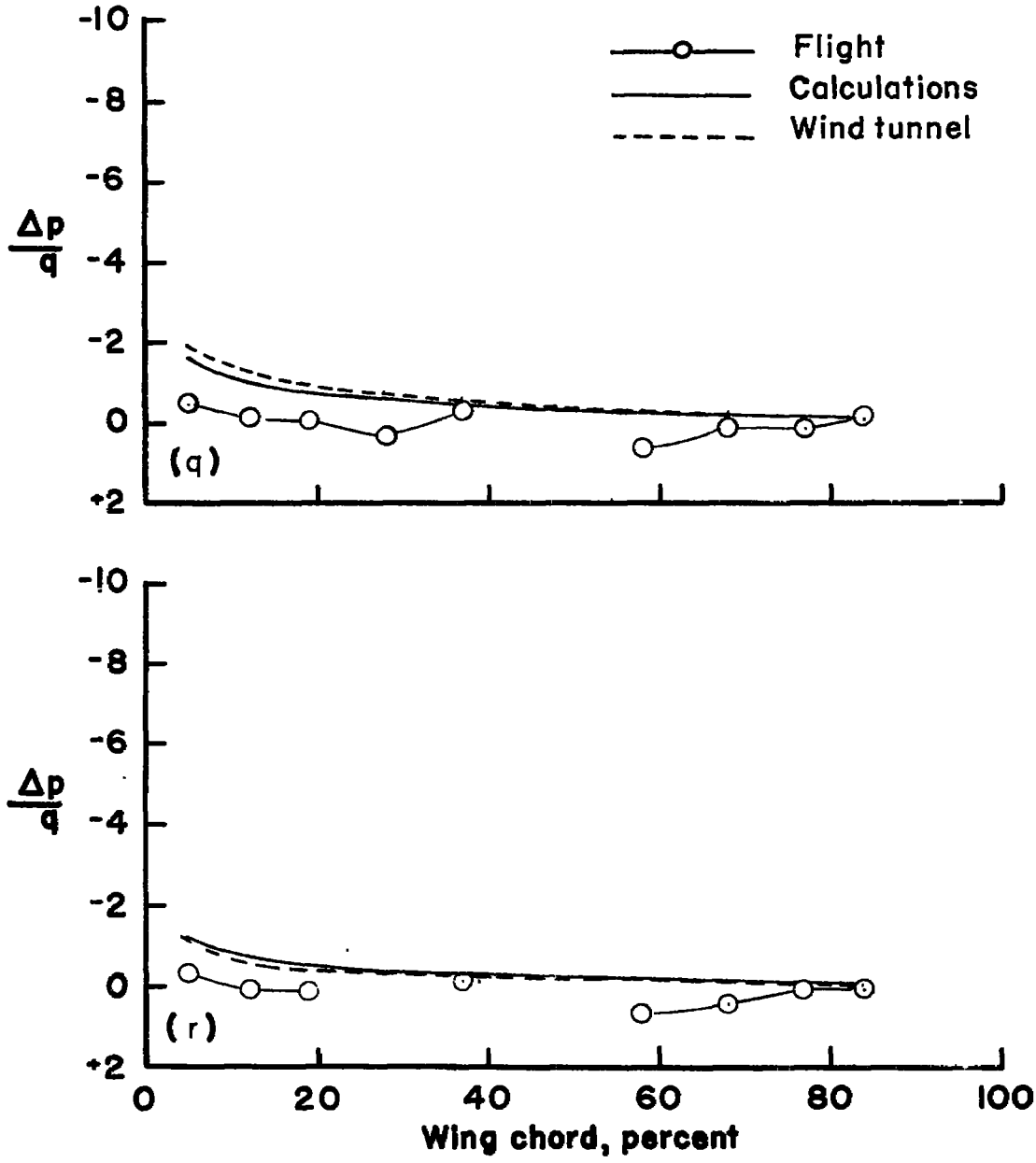

(q) Time, 19 milliseconds; $\alpha = 4.8^{\circ}$; distance, 3.38 chords.

(r) Time, 20 milliseconds; $\alpha = 3.8^{\circ}$; distance, 3.56 chords.

Figure 12.- Concluded.

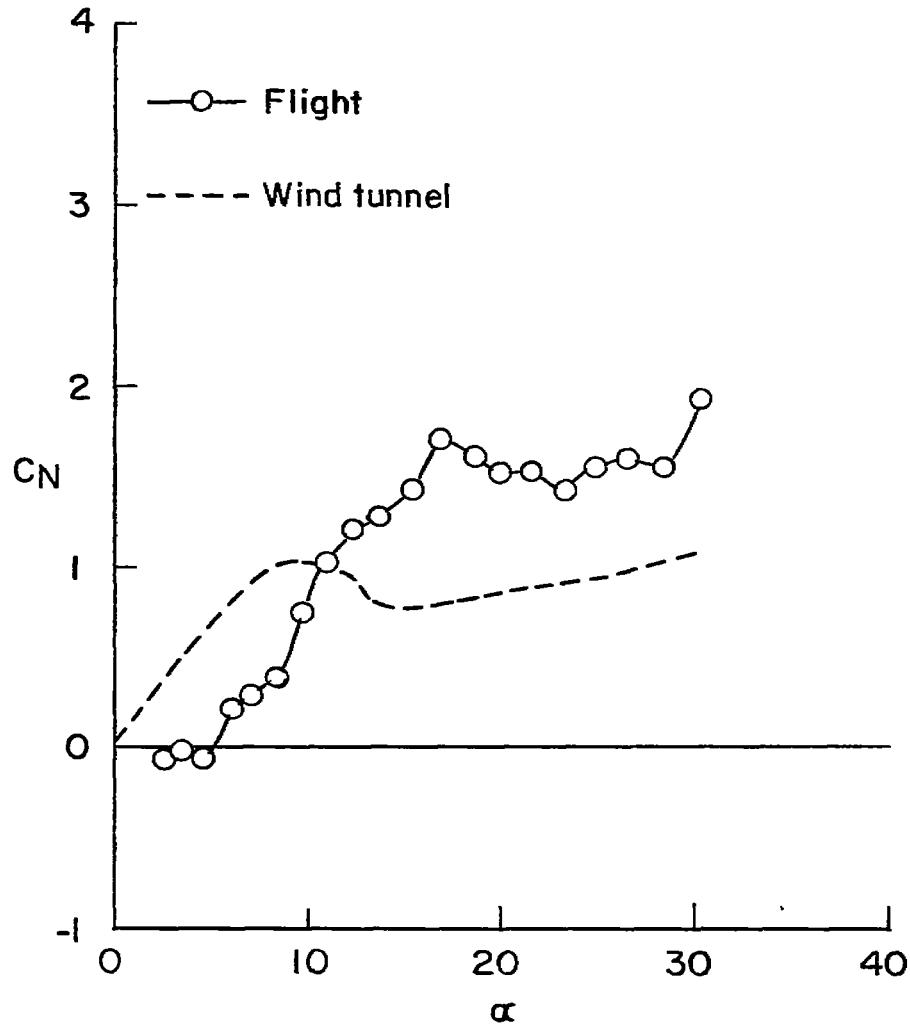

Figure 13.- Comparison of normal-force coefficients obtained from flight and wind-tunnel tests as a function of angle of attack.

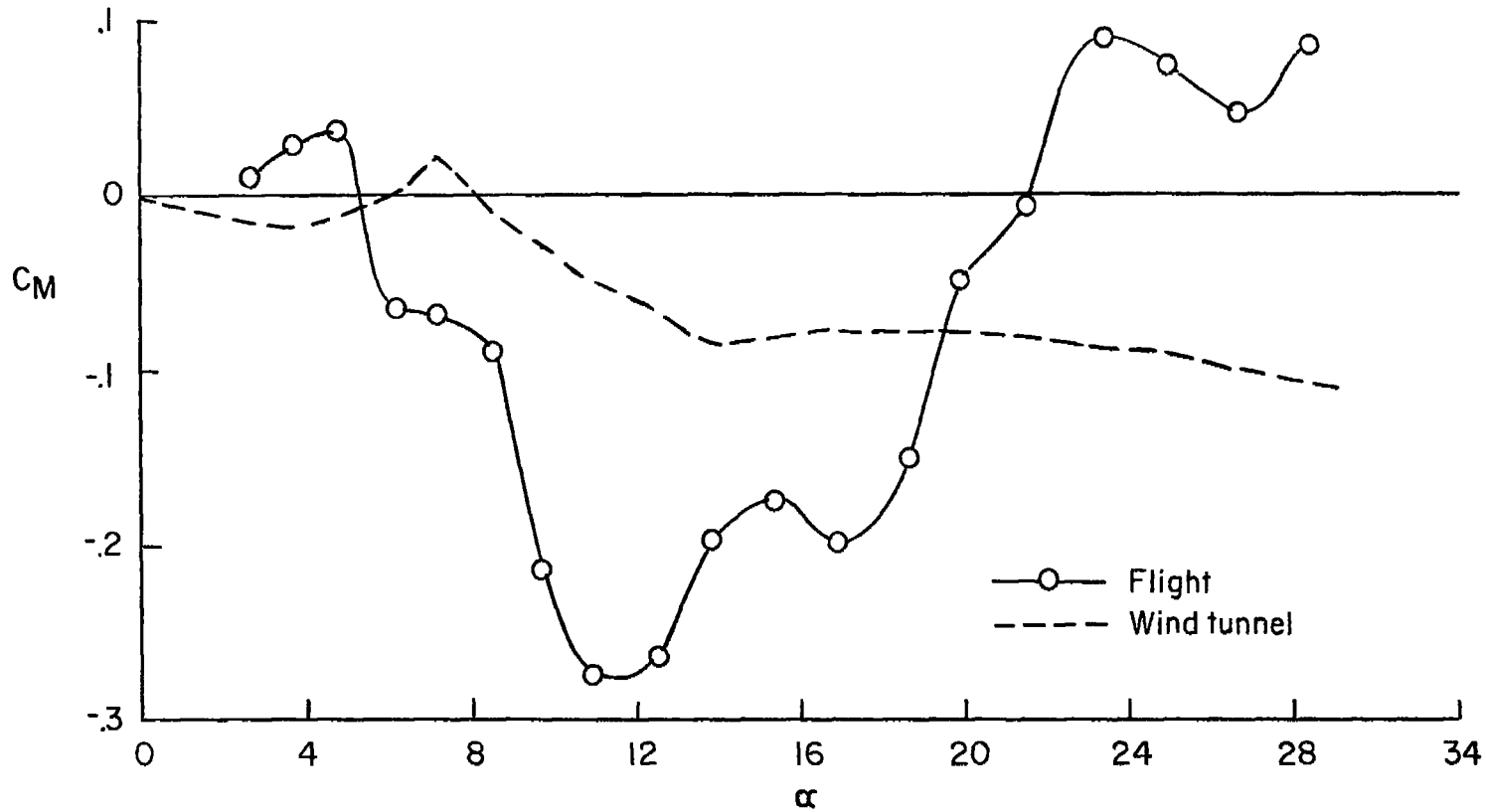

Figure 14.- Comparison of moment coefficients obtained from flight and wind-tunnel tests as a function of angle of attack.

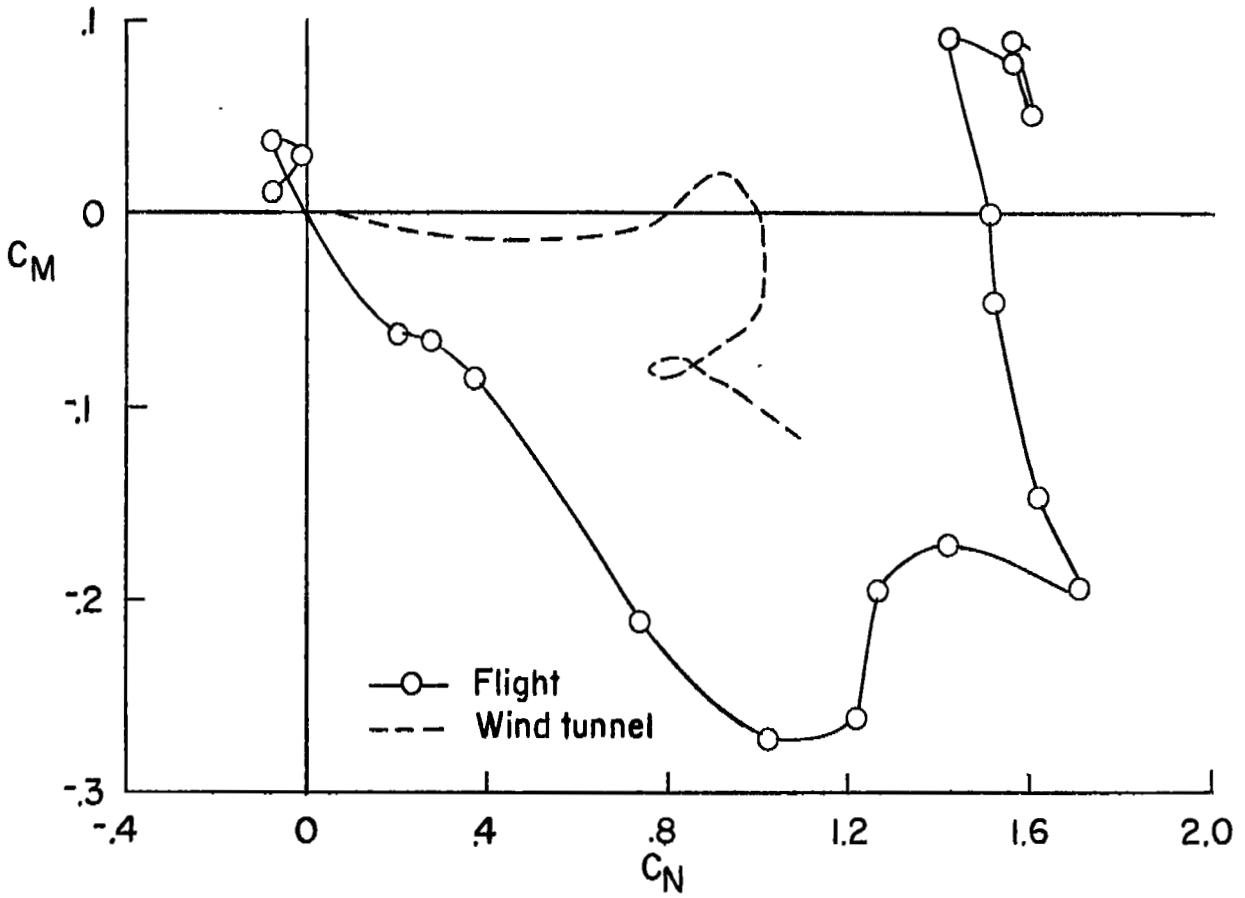

Figure 15.- Comparison of moment coefficients obtained from flight and wind-tunnel as a function of normal-force coefficient.

NACA - Langley Field, Va.